

Diffuse Interstellar Bands: A Comprehensive Laboratory Study
Fred M. Johnson
Cal State University Fullerton
Dept. of Physics, P.O. Box 6866, Fullerton, CA 92834, USA

Abstract

As a result of the search for the identity of the chromophores responsible for producing the diffuse interstellar bands, a comprehensive exposition of experimental data is presented, which implicates the following molecules: 1. The extremely stable organic molecules, magnesium tetrabenzoporphyrin (MgTBP) and H₂TBP. 2. A paraffin matrix (referred to as “grains”) containing TBPs. 3. A low concentration of pyridine (also within the grains), whose transmission window at 2175Å, accounts for the ubiquitous UV bump. The blue emission spectra associated with the central star, HD44179, of the Red Rectangle displays the fluorescence excitation spectra of *bare* MgTBP. This unique spectrum matches the low temperature lab data of MgTBP in the vapor phase. An effective grain temperature of 2.728 K (+/- 0.008) was deduced, based on MgTBP’s lowest measured vibrational state of 341 GHz.

Keywords: Diffuse interstellar bands; Porphyrins; Vibronic spectra; Shpol’skii matrices

1. Introduction

Since 1921, diffuse interstellar bands (DIBs) have presented an extreme challenge to both astronomers and spectroscopists. These bands are seen primarily in the spectroscopic data of distant, bright background stars, whose light has undergone multiple scattering associated with grains within intervening, interstellar clouds. The interstellar origin of DIBs was established by Paul Merrill [1]. At first, only a handful of these features were discovered, with one particular feature, the 4428Å DIB, being the most prominent. Several hundred DIBs are now being reported, a large number as yet unverified and unpublished. The quest for a solution to the DIB enigma has recently gained increased attention; its solution is regarded as potentially far-reaching in its implied cosmological significance.

G.H. Herbig [2] reviewed the historical background relating to the discovery of the DIBs, and discussed numerous proposals for their identification. The earliest summary of experimental work on the DIB enigma was presented in 1965, [3] concluding with the suggestion of complex hydrocarbon molecules as the carrier of the DIBs. Snow’s review article [4], emphasized the experimental search for gas-phase molecules, overlooking critical solid-state literature, which includes high-quality Shpol’skii spectral data [5-29].

The Shpol’skii technique [8] is unique in that it facilitates the expression of well-resolved vibronic spectra of complex molecules such as porphyrins and phthalocyanines in frozen paraffin

matrices. Moreover, Shpolskii spectral bandwidths are comparable to those of narrow DIBs, whose band widths are characterized as “diffuse” (in contrast to the sharp atomic spectral lines).

2. Proposed solution

The proposed solution to the DIB enigma utilizes the extensive and meticulously accumulated observations of Herbig [2, 30-36], survey data [37], and the Red Rectangle fluorescence emissions [38-39], plus 36 years of accumulated lab data of Magnesium-tetrabenzoporphyrin (MgTBP) (Fig. 1) and the free-base variety, H₂TBP [40-42]. These highly stable, abiotic molecules belong to a sub-class of a larger category of molecules known as, “porphyrins and metalloporphyrins” [43-45]. Porphyrins are extensively studied for their importance in biochemistry and biology. They have also held center stage in a large variety of photochemical studies where they serve as photosensitizers [46-51]. In fact, MgTBP has been used by Goedheer [52, 53] as a chlorophyll analogue.

Preliminary results have been given previously [5,6, 41-42, 54-63] (this paper supersedes, and amends all previous work on this subject). The two postulated DIB chromophores are within two special classes of organic compounds (grains) composed of the solvent pyridine and mixtures of paraffins. The primary assumption is that the main chromophores, MgTBP and H₂TBP, are situated within a set of grain types where the “A-type” produces the quasilines (via Shpolskii matrices) and the “B-type” produces the inhomogeneously broadened features. Overlapping vibronic transitions account for wider DIB line widths as well as for some of their enigmatic substructure line shapes. Factors such as, different experimental conditions and techniques, various equipment and technologies, and scientific contributions from others contributed to the 40-year quest for a unique solution.

3. Experimental techniques

A systematic spectroscopic survey of a large number of organic compounds [57] was performed on a Beckman DK9 spectrophotometer. Low-temperature absorption and fluorescence data collection utilized a ¾ m Jarrell Ash spectrometer (dispersion of 20Å/mm) and was recorded on 5”x 7” photographic plates. Light sources included a high intensity tungsten lamp, HeNe, Argon Ion and/or HeCd (4416 Å) lasers.

MgTBP samples were prepared according to Linstead [64], Koehorst et al. [65] by various chemists over a ten-year period. One sample was a gift from Dr. Frank Träger. The Shpolskii matrix isolation method [8] was attempted throughout, with the tetrabenzoporphyrin samples first dissolved in pyridine and then diluted with either n-octane, n-nonane or n-decane.

Sample thickness was varied from about one to five millimeters. Absorption data required exposures of the order of minutes, whereas fluorescence data would vary from 15 minutes to 5 hours. A typical run would be seven separate exposures recorded on a single photographic plate. About two-dozen CSUF physics undergraduates collaborated in the data collection. Preliminary Shpolskii data reported previously [41, 42] plus over 120 spectral plates were meticulously re-measured by Perry Rose. Some of the plates were recently rescanned by David Weinkle, using modern technology, in order to facilitate an improved spectral representation of the data.

Room temperature FTIR spectra were taken of Mg TBP using both reflection and transmission set-ups. Raman spectra of MgTBP was obtained via Dr. Markwort.

The Q-band $S_1 \leftarrow S_0$ region of “bare” MgTBP was measured by Dr. Brumbaugh at the University of Chicago. The laser induced fluorescence (LIF) spectra covered the optical region from 5650Å to 6165Å. MgTBP was first heated to 425°C to produce a vapor, which was subsequently cooled by means of a supersonic jet of helium.

Preliminary measurements of the $S_2 \leftarrow S_0$ transitions of “bare” MgTBP were taken by Dr. U. Even at Tel Aviv University. The experimental arrangement incorporates the following innovations:

- (a) Pulsed supersonic gas expansion and simultaneous molecular ion mass determination.
- (b) Molecular photo ionization is achieved by means of two synchronously pulsed laser beams, where one has a fixed and the other a variable frequency. Their combined energy was in slight excess of 7.3 e.v.

4. Results

The search originated with an earlier, unsuccessful experimental study at Columbia University involving F-centers in alkali hydrides [66].

Subsequent research involved absorption measurements of hundreds of diverse types of compounds, including a large variety of neutral polycyclic aromatic hydrocarbons (PAHs). The resulting spectra was inconsistent with the known DIB spectra [57]. In addition, an extensive library search provided the important clues, which led to the TBPs.

MgTBP is designated as the primary molecule. At room temperature [40] with MgTBP in a pyridine solution, the dominant spectral features are the Soret band at 4422Å, the Q band at 6344Å, the weaker Q (0, 1) broad structure at 5900Å and a vibronic structure at 4161Å. These features are far better resolved at temperatures of 77K and below, with slight temperature related spectral shifts. The peak of the 4422Å Soret shifts to 4428Å (and is weakly dependent on the pyridine/paraffin ratio); the 4161Å becomes 4175Å. The latter value is consistent with astronomical data by Herbig et al. [2, 67]. The Q (0, 1) and the Q bands show well-resolved structures, both in the lab and DIB data.

4.1 Lab quasiline Shpolskii spectra at 77K

The successful production of quasilines depends primarily on the paraffin solvents, on sample cooling rates and on the resulting microcrystalline structural environment in the vicinity of the MgTBP hosts. In addition, critical parameters include sample preparation, sample thickness, and the proper experimental techniques for producing and recording the spectra.

Mixtures were generally of arbitrary concentrations and, hence, resulted in a good diversity of absorption and fluorescence spectra. The Soret (4428Å) and Q-bands (about 6300Å), would generally be obtained as an inhomogeneous, broadened background [41, 42].

The following DIBs are isolated from the potential DIB list (on the basis of lab data, see section 4.5):

1. 6597Å, 6591Å, 6177Å, 4385Å, which are assigned to the free base derivative, H₂TBP .
2. 4882Å, which is tentatively assigned to a non-descript MgTBP fragment [5,6].

The remaining DIBs are tentatively assigned to MgTBP.

Shpolskii quasilines did not always materialize for MgTBP. At other times, different Shpolskii lines emerged depending on the “sites” that were generated upon cooling. A large amount of data collection was therefore needed in order to locate all possibilities. The accumulated Shpolskii lab data implies that on a purely random basis, a large variety of sites can arise [19-21, 24-26, 28, 68-71]. Possible variations include solvation, differing pyridine/paraffin ratios, different sets of paraffins, crystal structures, and chromophore configurations such as monomers, dimers, and with/without pyridine ligands attached to the central Mg atom.

Broad spectral features are indicative of the inhomogeneous case. Based on the 120+ lab experiments, at least five distinct sites associated with its lowest excited electronic state (S₁) occur most frequently. Figure 2 is a representation of the S₁ sites identified so far. The complete set of vibrational frequencies (Table 1), and the various identified electronic (0-0) origins of the S₁ and S₂ states, allow for decoding and identifying the majority of the reported DIBs.

Table 1 is a comprehensive listing of lab-measured vibrational frequencies of tetrabenzporphyrins plus magnesium porphyrin (MgP), measured under widely different physical conditions, and including a large amount of data accumulated from this work. MgP is the basic porphyrin structure, viz. MgTBP minus its four attached benzene rings. The referenced [26] vibrations of MgP listed in Table 1, column 12, thus apply solely to the basic porphyrin ring.

With the exception of referenced data by Platenkamp and Canters [7] and that of Sevchenko et al. [11], all Shpolskii quasiline spectra of MgTBP and H₂TBP in this manuscript were generated in the author’s laboratory. FTIR data was taken by the author in the CSUF chemistry lab (table 1, column 6).

Low temperature LIF spectra of bare MgTBP was commissioned (using the author’s MgTBP samples) and taken by Dr. D. Brumbaugh (Fig. 4) and Dr. U. Even (Fig. 8a.). This data is displayed in columns 1 and 2 of Table 1a.. MgTBP Raman data was obtained from Dr. Lars Markwort and Dr. Neal Spingarn (Tables 1, column 13). Dr. Spingarn also kindly supplied the reflection data for MgTBP (Table 1c onward). The purpose of this additional (so far unpublished) outside data was to lend support to the overall internal self-consistency of the extended list of vibrational frequencies listed in Table 1.

The set of possible vibronic transitions in MgTBP: S₁(v)←S₀, S₂(v)←S₀, produce a fraction of the observed DIBs. The DIBs in the red region originate from transitions S₀(v)←S₁(0). The strongest lab (Soret) band at 4428Å (Fig. 3) is also the strongest DIB. Its huge (lab) molecular extinction coefficient (1.5 x 10⁶) allows for interstellar abundance determination. There are 2 x 10¹⁴ MgTBP molecules per cm² in this line of sight for HD183143.

Table 2 lists all the lab-measured Shpolskii bands of MgTBP and the corresponding possible and definitive DIBs. It displays an overwhelming number of matches to the precision of the hand-measured data (about $\pm 1 \text{ \AA}$, consistent with spectral equipment resolution).

Tables 3 and 4 contain lab spectral data converted to wave numbers. Subsequent columns are the tentative, vibrational assignments compatible with entries from Table 1, connecting each transition to its respective origin, indicated at the top of each column. Each site has its own origins. For the S_2 state, the crystal field splitting is 35 cm^{-1} and only one site has so far been identified. The origins were derived and confirmed from the totality of entries of all measured vibronic transitions.

An abbreviated list of lab absorption and fluorescence spectral data is displayed in Table 4, which shows entries for both fluorescence and absorption lines near the Q band origin, taken under different experimental conditions. Each entry of a lab line is given a tentative assignment of an electronic origin, site and corresponding vibrational frequency, derived from Table 1. The overall data supports the MgTBP identification, since it involves highly reliable vibrational frequencies, in addition to the actual DIB matches. (The reliability factor arises from the multiplicity of independent measurements having equal or almost equal values).

The columns in each table describe the following: “n” represents the number of separate individual measurements, where the wavelength values in column two are average values. The most prominent DIB at 4428 \AA [72] and the superimposed lab data produce an exact match, see Fig.3. Note, both the wavelength and “base” band width match (see discussion in section 4.4 of the Soret band width). Representative MgTBP Shpolskii spectra (apart from Figs 3-6) can be found in several publications [7, 11]. Fig. 4 shows a lab band at 6379 \AA , which encompasses DIBs $\lambda\lambda$ 6379, 6376, 6362 and 6353. Additional representative Shpolskii spectral bands from this work are shown in Figures 5 and 6, where rescanned data from two and six separate plates, respectively, were superimposed.

4.2 The $S_1 \leftarrow S_0$ transition (bare MgTBP)

The data shown in Fig. 7 covers three different spectral regions, each having a different gain. Fig.7 shows the LIF spectra in the range 5650 to 6165 \AA of Mg TBP seeded in a supersonic expansion of helium. The intense peak at 6115 \AA is clearly the electronic origin (0-0) of the $S_1 \leftarrow S_0$ transition. The spectra displayed in Fig.7 are attributed to the electronic-vibrational excitations of the $S_1 \leftarrow S_0$ transitions, originating from the ground vibrational state of S_0 . The 0-0 band asymmetry may originate from unresolved vibrational sequence congestion, involving low-frequency vibrational modes, which were not effectively cooled, based on analogous observations by Fitch [73] on phthalocyanines. Table 1 compares the data of MgTBP with that of ZnTBP [74].

The inset of Fig.7 shows in greater detail the region close to 0-0. The ultra-low frequency modes are enhanced in this scan, which was taken under conditions of increased gain.

4.3 The $S_2 \leftarrow S_0$ transition (Soret region), of “bare” MgTBP

The experiment confirmed the molecular weight of 532 for the MgTBP ion and coincidentally showed that MgTBP is stable against spontaneous UV photodisintegration in the 7.3 e.v. energy range.

Fig. 8a shows a preliminary excitation spectrum of “bare” MgTBP in the spectral region of 3900 to 3960 Å. The data is designated “preliminary” because ultimate cooling of seeded MgTBP molecules in the pulsed, high pressure HeNe mixture was not attained due to a valve assembly fatigue. Fig. 8a, nevertheless, shows sufficient resolution of peaks, (superimposed upon vibronic congestion) to permit the identification of the electronic origin of the $S_2 \leftarrow S_0$ transition as 3945.6 Å, based on the fact that only one other intense peak was found (on the long wavelength side) on scanning up to 4000 Å. The 3947 Å peak arises from a vibrational level 11 cm^{-1} above S_0 (i.e. hot band) and thereby confirms the incomplete cooling in this experiment. Additional confirmation of this 11 cm^{-1} excited state level is found in (a) the isolated MgTBP molecule LIF spectra (Fig.7) and (b) a direct microwave, room temperature absorption measurement by Dr. P. H. Siegel [75] of JPL, which gave 341 GHz. (Fig.9). The latter value was confirmed by measuring its second harmonic at about 680 Ghz .

4.4 The Soret bandwidth and the $S_2 \leftarrow S_0$ transitions of MgTBP in a frozen matrix

Table 3 lists measured quasilines, plus the Soret band associated with the $S_2 \leftarrow S_0$ vibronic transitions of MgTBP in pyridine/paraffin matrices at 77K. The number of independent measurements (n) is indicated in column 1. The origins, S_{2x} and S_{2y} were determined to be 22,444 and $22,479 \text{ cm}^{-1}$ respectively. Additional confirmation of the 35 cm^{-1} splitting is obtained by 25 vibrational assignments, including three pairs of quasilines, whose average energy separation is 34.3 cm^{-1} .

Note that the Soret band in Table 3 (shown schematically in Fig. 10) is not coincident with either of the electronic origins but 139 cm^{-1} above the S_{2x} state instead. It is postulated here that the unusually high intensity of the Soret band and its apparently irreducible vibronic bandwidth at 4K, (Fig. 8b) arises from the superposition of (possibly 17-36) vibronic transitions. This could comprise most of the measured vibrations from 11 to 247 cm^{-1} . There are 36 vibrations listed in Table 1a, which fall in this range.

The base band width of the important $\lambda 4428$ DIB can be deduced from two independent results: (a) MgTBP, in a single crystal of n-octane at 4K [7] produced a Soret base band width of 279 cm^{-1} (Fig. 8b), (b) the isolated MgTBP molecule scanned near its S_2 origin revealed a 244 cm^{-1} wide base due to fortuitously insufficient cooling (Fig. 8a), thereby producing vibrational congestion. In the matrix, one has to add 35 cm^{-1} (crystal field splitting) to the measured 244 cm^{-1} congested region to produce an effective base width (Δ) of 279 cm^{-1} . Therefore, both sets of results (a) and (b) are consistent with the DIB base band width of 51 \AA (279 cm^{-1}) for the $\lambda 4428$ DIB [30, 76]. It also confirms the 139 cm^{-1} displacement of the peak of the Soret band (to $\pm 1 \text{ cm}^{-1}$) from the 0-0 origin (Fig 10).

Exact coincidence of both the peak wavelength of the $\lambda 4428.2$ DIB and the MgTBP lab data, plus its base band width make a compelling case for the chromophore identification. Note, in particular, that the base band width is independent of interstellar scattering and possible DIB saturation. Further confirmation for the correct assignments for the double origins of the S_2 state (viz. $22444, 22479 \text{ cm}^{-1}$) can be seen in Table 5, where a large number of reported and probable DIBs in the blue spectral region are listed. The vibrational frequencies from Table 1, appropriate for each of the vibronic transitions are tabulated in columns 4 and 5. Note the special cases of wide band DIBs, $\lambda\lambda 4595$ and 4760 . The listed, multiple, superimposed vibronic transitions reproduce both the correct observed band width *and* their *average values* match the measured DIB central peak wavelength.

New possible DIBs (tabulated in Table 5) were derived from measurements of unassigned (or incorrectly assigned) absorption bands in the quoted references. In the future, an additional criteria for DIB identification could be the method outlined above, whereby vibronic assignments (based on the code) could be the final determining factor. Several identical vibrational frequencies are involved in the production of vibronic transitions from each of the origins S_{2x} and S_{2y} respectively. The three pairs in Table 5 are ($4394, 4401 \text{ \AA}$), ($4413, 4420 \text{ \AA}$) and ($4381, 4525.5$). Since vibrational frequencies in Table 1 are unique to the TBPs, their exact match in the vibronic transitions provides additional evidence for the MgTBP identification.

4.5 The H_2 TBP molecule

4.51 The Soret Band of H_2 TBP

The lower extinction coefficient (relative to MgTBP) [40] of the Soret band in H_2 TBP at $\lambda 4385$ (Fig. 11) must be attributed to its lack of intrastate vibrational coupling. This would suggest that the central Mg atom plays an essential role in promoting (or facilitating) intrastate coupling, which, in turn, would produce the strongly enhanced Soret intensity in MgTBP. There is evidence for the presence of the relatively weak 4385 \AA band in some of the published high S/N spectra [30].

4.52 The Q-Bands of H_2 TBP

Fig. 11 shows a non-Shpol'skii absorption spectrum of H_2 TBP at 77K. It displays the 4385 \AA Soret band and the double Q bands. The band at 6592 \AA corresponds to the probable DIB identified by Herbig [2] at 6591 \AA . The other broader, irregular lab feature has an average value of 6177 \AA . and would correspond to a broad DIB at that wavelength [2]. Fig. 7 by Johnson [42] displays a well-resolved vibronic spectrum of H_2 TBP, establishing an unambiguous identification of one of the (0-0) origins at 6597 \AA and providing an exact DIB match. Fig. 6 in Johnson [42] is an absorption spectrum of H_2 TBP, displaying four of the multiple Shpol'skii bands, previously referenced, as well as a band at 6174 \AA . This band would correspond to the (29 \AA FWHM) wide DIB at 6177 \AA [2]. The identical H_2 TBP spectrum (plate #201) is also shown in Fig. 4 of Johnson [41] (it was erroneously mislabeled as molecule χ). Thus, since the principle absorption bands of H_2 TBP can be matched with their DIB counterparts, this molecule is assigned as one of the interstellar grain constituents.

4.6 The UV Bump

The 1964 discovery of a so-called UV bump at 2175Å [77] has been followed by a substantial amount of astronomical data [78-82] and parametric analyses [83]. However, no convincing experimental lab data had ever been previously presented or published. The important clue, which led to its ultimate identification in 1994 [6], was the correlation of this bump with the strength of the 4428Å DIB [84-85].

The 2175Å bump appears in the astronomical data as an absorption feature, whereas, it is, in fact, a transmission window between two very strong absorption bands of pyridine [86]. To demonstrate this experimentally at room temperature, a 10 cm long quartz cell filled with octane was used and a single drop of pyridine added. The result is shown in Fig.12. A typical UV bump superimposed on the lab data is shown in Fig.13.

Hence, the UV bump originates as a result of trapped energy (in the 2175Å band) within the interstellar grains, and becomes apparent as “missing energy” (absorption) as a result of multiple scattering processes. A fluffy interstellar grain, having pyridine content, would allow a partial penetration of incoming stellar radiation in the 2175Å band, which, unlike the case of a liquid medium, would not necessarily reemerge from the grain and thus be absorbed. Preliminary results of this experiment were reported previously [6]. Variability of UV bump bandwidths in different lines of sight, are directly related to the variability of pyridine concentrations in the grains.

4.7 Fluorescence

Prior to 1975, DIBs had never been seen in emission. There are now a significant number of examples of DIB emissions. These include two in some O-type stars [72] and at a minimum three towards HD29647 [84, 85], plus a large number of emission bands from the RR [87].

4.71 The special case of HD29647

The DIBs in HD29647 need further elaboration. As was pointed out previously [5], the unusually sharp DIBs (some of which are in emission) in this line of sight, are assigned to MgTBP molecules situated in matrices, which are essentially devoid of pyridine. Hence, they may be analyzed based on the work of Platenkamp and Canters [7], where these molecules were imbedded in a single crystal of n-octane at 4K, and their spectra recorded from a single site. Table 6 lists ten of these DIBs and their assigned vibronic transitions from origins 15962 and 15992 cm⁻¹, respectively. Fig. 14 is a copy of the original data [88] on which the characteristic 30-31 cm⁻¹ separation is shown, indicative of the S₁ crystal field splitting for site VI (Fig 2).

4.8 The Red Rectangle (RR)

The correspondence between RR emission features and DIBs, was pointed out by Fossey [89] and Sarre [90]. MgTBP lab data (Table 2) confirms 35 out of a possible 57 RR bands [39]. Based on observations by Scarrott et al. [91], it was revealed that RR emission profiles of λ5797Å,

5850Å and 6614Å change with distance from the central excitation source HD44179. Van Winckel et al. [87] provided a detailed analysis of these RR emission features. Fig. 15 (modified from Fig. 9, Van Winckel [87]) suggests that there is a ready explanation for the apparent discrepancy between the RR features and DIBs based on the measured vibrational spectra of MgTBP. It should be noted that Glinski and Anderson [92] also measured RR emission in the 5800Å region as a function of distance from the star and were, likewise, aware of the apparent RR wavelength offset from the 5797.11Å DIB.

4.81 Resolution of the apparent RR vs. DIB discrepancy

Note, in Fig. 15, that if one extrapolates the measured peak wavelengths as a function of distance to the star, the lower line (designated “A” for the 5797Å DIB) intersects at 5801Å. This corresponds to a difference in energy from the 5797.11Å DIB of 11.3 cm^{-1} . Similarly, for the lower panel, extrapolation to the star yields 5853.7 Å, which corresponds to an energy difference from the 5849.78Å DIB of 11.3 cm^{-1} . This value corresponds to the lowest measured vibrational frequency of MgTBP!!

The other extrapolation to the star yields 5818Å (line “B”). This corresponds to an energy difference of 62 cm^{-1} (see Table 1a) from the 5797.11Å DIB.

For the lower panel of Fig. 15, extrapolations C, D and E intersect at the zero arc distance at 5856.2Å, 5859.3Å and 5861.3Å, respectively. This would correspond to vibrational frequencies, 18, 28 and 33 cm^{-1} of MgTBP, (Table 1a).

Table 7 is an abbreviated extension of Table 4, listing potential “sites” and the corresponding frequencies (from Tables 1e and 1f) that are associated with the vibronic transitions for DIBs 5797.11 and 5849.78Å. The reason why the 62 cm^{-1} vibration is favored for 5797Å may be related to the fact that three pairs of transitions have energy differences of 62 cm^{-1} . These pairs are: (1333 and 1271); (1400 and 1338) and (1437 and 1375) cm^{-1} respectively.

Similarly, the lower panel contains the following pairs of values: (1186,1153); (1212,1184) cm^{-1} , whose energy differences are 33 cm^{-1} and 28 cm^{-1} , which correspond to the extrapolated intercepts E and D, respectively.

It is obvious that the closer the distance to the star, the greater the photon light intensity and, hence, a proportional increase in optical-pumping efficiency and an increased population of low lying vibrational levels.

4.9 Discovery of hot, isolated (bare) MgTBP molecules in the RR nebula.

The blue spectral emission features, extending from 3700 to about 4500Å, had previously been attributed [93] to be scattered light from the central star HD44179. A re-examination for the purpose of this paper, resulted in an unexpected discovery. These features reveal an extended emission spectrum, which in fact, can be unambiguously assigned to the fluorescence excitation spectrum of bare MgTBP, displaying well-resolved vibrational excitations of the Soret band. The

spectral feature with the greatest intensity is located at 3945.6 Å, which corresponds to the electronic origin (0-0) of the $S_2 \leftarrow S_0$ transition of MgTBP (Fig. 16 and lab data, Figs. 8a.).

The wide band width of these features implies vibronic congestion (see section 4.3) characteristic of a high temperature environment. These elevated temperatures in turn produce a Boltzmann distribution of excited vibrational levels of the S_0 ground state. The resulting so-called "hot bands," seen in the RR emission spectra, extend to about 4300 Å. Table 8 lists the wavelengths of all the blue emission features measured from the original RR spectra (Fig. 16, adapted from Fig. 1 in Schmidt et al [93]). The electronic S_2 state of MgTBP in the vapor phase is doubly degenerate. Hence, there is only a single 0-0 origin ($25,344.7 \text{ cm}^{-1}$). A vibrational analysis is shown in Table 8 where the vibronic transitions originating from $S_2(0) \leftarrow S_0(v)$ and $S_0(v) \leftarrow S_2(0)$ are listed.

Note in Table 8, that a pair of vibrations (402 and 619) are symmetric about the 0-0 origin, with another set (401 and 617) in the hot band vibrational sequence. A total of 15 vibronic transitions are listed, whose frequencies are well established for MgTBP (see Table 1), thus, adding considerable weight to the MgTBP identification. Errors in measuring the blue RR emission bands are of the order of 1-2 Å. Hence, one has to allow for a $\pm 3 \text{ cm}^{-1}$ range in assigning vibrational frequencies. The distribution of maximum peak intensities (I_p) of the hot bands can be used to determine an effective Boltzmann temperature for the MgTBP molecules. A plot of $\log_e(I_p)$ vs. excitation energy (Fig. 17) provides an effective excitation temperature of 1580 K. The probability that any other organic molecule (other than MgTBP, which sublimates) can tolerate and/or survive this apparently high temperature regime is very low.

5.0 Theory

The two chromophores MgTBP and H_2 TBP have spatial symmetries, which place them in point groups D_{4h} and D_{2h} , respectively. For the former, Gouterman's [94] four-orbital model predicts a degenerate $S_1 \leftarrow S_0$ transition (Q-band) and a degenerate $S_2 \leftarrow S_0$ transition (Soret or B band), where both transitions are polarized in the molecular plane. The degeneracy of the excited states in MgTBP can be lifted by the action of a crystalline field that may originate within solids such as a Shpol'skii host matrix or a single crystal.

The strong Soret and Q bands arise in part from the delocalized nature of the Π electrons shared by the 16 or 18 conjugated bonds in the ring. The Q band transition is made possible by configuration interaction mixing.

Since a large number of DIBs consist of overlapping vibronic transitions, the intensity (I) of each DIB resulting from such a combination is given by

$$I = \sum_i n_i m_i p_i q_i$$

Where,

- n= number of crystal sites involved in the line of sight
- m= transition probability for each vibronic transition
- p= probability that a certain site is occupied

q=probability that a certain configuration (chromophore and lattice) is involved

An experimental measure of the p factor is obtained by the number of times a particular transition is observed in the lab spectra, and is indicated as such in the lab data.

A large number of DIB vibronic transitions involve identical vibrational frequencies. The latter implies that the nuclear potential surfaces in the S_0 and S_1 states are essentially identical, which is independently confirmed by various lab measurements on the TBPs.

The data reported here confirm some of the vibrational modes associated with the analogous zinc-tetrabenzoporphyrin, specifically related to the pyrrole structure, viz. 746-752 cm^{-1} and 966-978 cm^{-1} , where the latter corresponds to the pyrrole breathing mode. The in-phase C_aC_m stretching mode of A_{1g} symmetry (D_{4h} notation) reported for ZnTBP [95-96] at 1620 cm^{-1} is also present in MgTBP. Other reported vibrations for ZnTBP are 1584,1520,1379,1335,1320 and 1235 cm^{-1} have corresponding frequencies in MgTBP at 1585,1518,1374,1336,1321, and 1235 cm^{-1} respectively, corresponding to the symmetric vibrations of the isoindole subunits.

The fact that both MgTBP and ZnTBP show vibrational modes that differ only by one or two wave numbers, is not unexpected, since the central metal plays only a very minor role in most of the fundamental frequencies of these tetrabenzoporphyrins. The pyrrole symmetric half ring stretching frequency is split into modes 1374 and 1335 cm^{-1} for MgTBP, with the higher frequency mode localized primarily on the benzo rings. Bands 1132-1136 cm^{-1} correspond to the C_mH in-plane bending mode. Bands 1313-1321 cm^{-1} correspond to the stretching frequency mode of C_aN . The 11.3 cm^{-1} vibration is associated with the bending modes of the four outermost benzene rings [97].

Theoretical transition probabilities for fluorescence of vibronic bands, originating from a typical S_1 electronic state, are of course, quite different than transition probabilities for absorption from the ground state, S_0 . This fact can be readily seen in the experimental data [7]. To date, unidentified infrared (UIR) emission bands are routinely being compared with e.g. PAH molecular absorption data, rather than the appropriate fluorescence transition probabilities, or fluorescence lab data.

6.0. The Interstellar Grain Temperature

Assume that the lowest vibrational energy of MgTBP ($\nu = 341$ GHz) (See Figure 9) is transferred to the phonon vibrational modes of its host crystal lattice (paraffin matrix). The laws of thermodynamics [98] provide the following equation:

$$\frac{1}{2} NkT = h\nu$$

where N is the number of degrees of freedom of the four (n) outermost benzene ring bending modes, plus the 2 pyridine molecules attached to the central Mg atom, giving a total value for

$n = 6$. The Boltzmann and Planck's constants, k and h respectively, are well - known. Thus, $N = 3n - 6$ and since $n = 6$; $N = 12$.

Substituting all known and measured values, gives

$$T = 2.728 \text{ K } (\pm 0.008)$$

This implies that grains containing MgTBP would essentially radiate as black bodies at an equivalent temperature of 2.728 K. This is the temperature attributed to the cosmic background radiation, and hence has the potential to negate the Big Bang Theory.

7.0 Discussion

Weak DIBs seen as substructures by Krelowski and Sneden [99] and others are not only consistent with the proposed solution outlined in this paper, but seem to verify it in detail.

7.1 DIB Absorption vs. Emission

The processes by which the DIBs are generated in the interstellar medium (ISM) have to be reexamined. We are dealing primarily with a frequency sensitive multiple scattering phenomena. Based on the UV bump identification and the observation of isolated ISM DIB emission features, rather than absorption, provides the important forensic clue that one has to consider in detail the scattering process for each grain. Frozen paraffins have a white, fluffy, snow-like appearance, hence incident radiation may simply scatter or else has an opportunity to get trapped. Fluorescence or phosphorescence radiation generated within such fluffy cocoon structured grain material will be substantially trapped. Likewise, resonant radiation arising from the S_1 state will also be trapped, thus in effect lengthening the S_1 lifetime. Subsequent radiation of frequency $\nu_s = [S_1(0) - S_0(\nu)]/h$ would stimulate the emission of a photon from the S_1 state. Consequently, incoming radiation at frequency ν_s would, likewise be absorbed and be represented in the DIBs spectra as a missing (absorption) band in the multi-scattering process.

Transitions of the type $S_0(\nu) \leftarrow S_1(0)$ are generally seen in the ISM as absorption, however they are observed as fluorescence in the RR. Therefore, one may deduce that some grains in the RR are small (and probably young), and did not as yet coalesce to form the relatively larger, fluffy grain aggregates, which are presumed to be predominantly prevalent in the ISM. Fluffy grain particles [100] had been analyzed from the point of view of scattering theory, but not for their relevant implications to interstellar spectroscopy.

7.2 The DIB-grain Connection

In general, DIB strength, according to Herbig [34] is related (with some exceptions) to color excess, which implies a close association with grains. There are, however, an additional six, more cogent reasons why DIB chromophores have to be within grains.

1. Line widths consideration: in supersonically cooled, “bare” molecules [74] and this paper (Fig.7), vibronic lines have widths of the order of 1 cm^{-1} , which are extremely narrow, and therefore are inconsistent with the observed DIB line widths. Free molecules in interstellar space cannot readily produce, with precision, the wide range of observed DIB bandwidths despite the many valiant and unsuccessful attempts by Herzberg [101-103] and his successors. Note: Intrinsic line widths of interstellar atomic and diatomic spectral lines are invariably sharp and narrow, and never diffuse.
2. In special Shpolskii [8] type matrices, narrow lines are indeed produced, which are comparable in width to those observed in some of the narrow DIBs [2]. Wider DIB lines arise from overlapping vibronic transitions (see examples in Table 5) or inhomogeneously broadened lines. Use of the “code” (i.e. Tables 1+ and Fig.2) would extend this number to encompass virtually all of the DIBs.
3. Free molecules cannot readily account for specific transitions of DIB absorption in the interstellar medium and their appearance as fluorescence in the Red Rectangle spectra.
4. There are 15 pairs of DIBs [36] (and possibly more), which display the characteristic, crystal field-induced splitting (whose average value is 35.6 cm^{-1}) of the otherwise degenerate S_1 electronic state. This is consistent with MgTBP matrix lab data, and reconfirms the “inside grain” hypothesis.
5. Among the multitude of $35\text{-}36 \text{ cm}^{-1}$ wide DIB pairs, is the important Q-band duo of site I, viz. $\lambda\lambda 6284$ and 6270 (Fig. 5 and Table 4).
6. A total of well over 100 DIBs have so far been matched with the lab Shpolskii data to $\pm 1 \text{ \AA}$ [see Table 2]. The Shpolskii matrices would correspond to the solid state grains.

7.3 An Unintended Confirmation

Sevchenko [11] produced a set of (Shpolskii) quasilines of MgTBP in a pyridine-acetone-paraffin matrix at 77 K. Of the 14 lines shown in his spectra, six match the DIBs to a precision of 1 \AA . With the aid of the “code”, i.e. Tables 1+ and knowledge of the S_1 sites (Fig.2), each of his lines belong to a single site S_1 ($15,918 \text{ cm}^{-1}$). It should be pointed out that Sevchenko [11] was unaware of both the crystal field splitting and the relationship to the DIB problem. Moreover, Sevchenko did not explore the Soret region of MgTBP, hence the absence of the 4428 \AA band in his spectra.

7.4 Implications and Related Issues

Johnson, Bailey and Wegner [58] considered the interstellar synthesis of MgTBP. Cosmochemical evolution of large organic molecules was analyzed and addressed by Hodgson [104-108], with particular emphasis on porphyrins, using plasma synthesis technology.

Containment within a grain matrix retards the TBP destruction in the harsh interstellar environment [109]. However, its ultimate demise does lead to about 19 possible molecular fragments [59] already identified by microwave techniques [110-111]. Among these relevant, lab-measured fragments, is the unique interstellar molecule, MgNC [112]. Thus, the origin of this enigmatic radical is no longer a mystery.

Implications of this identification were considered: vis a vis cosmology and the origin of life [113, 114]. It might also be of astronomical interest that MgTBP molecules are paramagnetic in their S_1 singlet state [7, 29] and thus may contribute to (or be the source of) the weak postulated interstellar magnetic fields.

Extensive searches for *polarization* of DIB signatures have so far proved illusionary. This is consistent with the hypothesis that multiple scattering within the fluffy grain cocoon would vitiate any such chromophore signals. A substantial amount of high-quality Shpolskii spectral data (see the extensive list of cited references, originating largely from the Russian and Dutch workers) is clearly at variance with theoretical predictions [115-116] that profile variations, such as emission wings, are to be expected if the DIB features were created by impurity absorbers in grains. These theoretical predictions, which apparently do not apply to Shpolskii matrices, have unfortunately proven a major stumbling block to progress in this field.

8.0 Conclusions

The five characteristics that distinguish MgTBP and H₂TBP from other organic compounds are:

- (a) Thermodynamic stability (they sublime at 500° C).
- (b) Unique spectra (both wide and narrow lines depending on matrix).
- (c) MgTBP's Soret band, at 4428Å, has an extremely large molar extinction coefficient ($\sigma = 1.5 \times 10^6$).
- (d) Approximately 200 vibrations of MgTBP (which account for its stability), plus the doublets of five or six potential S_1 electronic "sites", are capable to produce a large number of potential vibronic transitions. This would result in a plethora of possible DIBs, predominately located in the red spectral region.
- (e) MgTBP is a highly efficient emitter of fluorescence radiation, specifically in the red spectral region, with photo-excitation in the blue spectral region.

An effective grain temperature was deduced from MgTBP's measured lowest vibrational state of 341 GHz: it is 2.728 K (+/- 0.008). This implies that grains containing MgTBP would essentially radiate as black bodies at an equivalent temperature of 2.728 K. This is the temperature attributed to the cosmic background radiation, and hence has the potential to negate the Big Bang Theory.

The combined weight of all the data collected in this paper points to one simple and unique conclusion. The success of critical scholarship and a diversity of relevant spectroscopic research is a quintessential demonstration of the compelling quality of Occam's razor.

Acknowledgement

Among the many outstanding CSUF physics students who participated in the spectroscopy were John Anthes, John Kerns, Ph.D., Mr. W. Krone-Schmidt, Mrs. L. Krone-Schmidt, Perry Rose, Anne Arroyo, Roberto Razo and Graciella Flores. David Weinkle took on the arduous task of rescanning Shpolskii data of a large number of photographic plates, utilizing his upgrades of a Jarrell Ash scanning densitometer. The generous scientific contributions of the following scientists are hereby most gratefully acknowledged: Dr. Don Brumbaugh, Dr. Benny Ehrenberg, Dr. Uzi Even, Dr. George Herbig, Dr. Lars Markwort, Dr. Franz-Peter Montforts, Dr. Roelof Platenkamp and Dr. Frank Träger. I wish to thank, in particular, Dr. Peter Siegel of JPL for providing the important mm microwave absorption measurement of MgTBP. Thanks as well to Dr. Neil Spingarn for supplementing Table 1 with new Raman and Reflection data. Helpful suggestions by the anonymous referee are appreciated and resulted in improving this manuscript.

References

- [1] P.W. Merrill, *Publ. Astron. Soc. Pac.* 46 (1934) 206.
- [2] G.H. Herbig, *Ann. Rev. Astrophys.* 33 (1995) 19-73.
- [3] F.M. Johnson in: J.M. Greenberg and T.P. Roark (Eds.), *Interstellar Grains*, NASA SP-140, 1967, p. 229-240.
- [4] T.P. Snow, *Spectrochim. Acta Part A* 57 (2001) 615-626.
- [5] F.M. Johnson in: A.G.G.M. Tielens and T.P. Snow (Eds.) *The Diffuse Interstellar Bands*, Kluwer Academic Publishers, Boston, 1995, p. 341-347.
- [6] F.M. Johnson, in: A.G.G.M. Tielens (Ed.), *The Diffuse Interstellar Bands: NASA Conference Publication 10144*, 1994, p. 47-51.
- [7] R.J. Platenkamp, G.W. Canters, *J. Phys. Chem.* 85 (1981) 56-63.
- [8] E.V. Shpolskii, A.A. Ilina and L.A. Klimova, *Dokl. Akad. Nauk SSSR* 87, (1952) 935.
- [9] R.I. Personov, *Optika I Spektroskopiya* 15 (1962) 61-71.
- [10] S.F. Shkirman, K.N. Solov'ev, *Investia Akad. Nauk SSSR* 29 (1965) 1385; also *Dokl.* 10 (1965) 349.
- [11] A.N. Sevchenko, K.N. Solov'ev, A.T. Gradyushko, and S.F. Shkirman, *Sov. Phys.-Dokl.* 11 (1967) 587-590.
- [12] E.V. Shpolskii, *Usp.Fiz.Nauk* 77 (1962) 321, *Soviet Phys.-Usp.* 5 (1962) 522.
- [13] P.E. Fielding and A.W.H. Mau, *Aust. J. Chem.* 29 (1976) 933-940.
- [14] J.E. Zaleskii, V.N. Kotlo, A.N. Sevchenko, K.N. Solov'ev and S.F. Shkirman, *Dokl. Akad. Nauk SSSR* 18 (1973) 320-322.
- [15] J.E. Zaleskii, V.N. Kotlo, A.N. Sevchenko, K.N. Solov'ev and S.F. Shkirman, *Dokl. Akad. Nauk SSSR* 19 (1975) 589-591.
- [16] F.F. Litvin and R.I. Personov, *Sov. Phys. Dokl.* 6 (1961) 134.
- [17] E.B. Karavaeva, B.D. Berezin and T.I. Potapova, *Zhur. Prikladnoi Spektroskopii* 32 (1980) 512.
- [18] N.M. Ksenofontova et al, *Zhurnal Prikladnoi Spektroskopii (J. App. Spectros, Eng. Transl.)* 20, 5 (1974) 834.
- [19] G.W. Canters, J. van Egmond, T.J. Schaafsma, and J.H. van der Waals, *Mol. Phys.* 24 (1972) 1203-1215.
- [20] G.W. Canters, G. Jansen, M. Noort, and J.H. van der Waals, *J. Phys. Chem.* 80 (1976) 2253-2259.
- [21] G.W. Canters and J.H. van der Waals, in: D. Dolphin (Ed.), *The Porphyrins*, Vol. III, Academic Press 1978, pp. 531-582.
- [22] J.A. Kooter and J.H. van der Waals, *Molec. Phys.* 37 (1979) 997-1013.
- [23] T.R. Koehler, *J. Chem. Phys.* 72 (1980) 3389.
- [24] G. Jansen, M. Noort, G.W. Canters, and J.H. van der Waals, *Molec. Phys.* 35 (1978) 283-294.
- [25] G. Jansen, M. Noort, N. van Dijk, and J.H. van der Waals, *Molec. Phys.* 39 (1980) 865-880.
- [26] G. Jansen and M. Noort, *Spectrochim. Acta, Part 32 A*, (1976) 747-753.
- [27] I.Y. Chan, W.G. van Dorp, T.J. Schaafsma, and J.H. van der Waals, *Molec.*

- Phys. 22 (1971) 741-751.
- [28] M. Noort, G. Jansen, G.W. Canters, and J.H. van der Waals, *Spectrochim. Acta*, 32A (1976) 1371-1375.
- [29] J.H. van der Waals, W.G. van Dorp, and T.J. Schaafsma in: D. Dolphin (Ed.), *The Porphyrins, III*, Acad. Press London, 1979, pp. 257-312.
- [30] G.H. Herbig, *Z. f. Astrophys.* 64 (1966) 512-517.
- [31] G.H. Herbig in: H. van Woerden (Ed.), *Radio Astronomy and the Galactic System*, IAU Symp. 31, 1967, p. 85.
- [32] G.H. Herbig, *Astrophys. J.* 196 (1975) 129-160.
- [33] G.H. Herbig, *Astrophys. J.* 331, (1988) 999-1003.
- [34] G.H. Herbig, *Astrophys. J.* 407 (1993) 142-156.
- [35] G.H. Herbig, and D.R. Sonderblom, *Astrophys. J.* 252 (1982) 610-615.
- [36] G.H. Herbig, and K.D. Leka, *Astrophys. J.* 382 (1991) 193-203.
- [37] P. Jenniskens, and F.-X. Desert, *Astron. Astrophys. Suppl.* 106 (1994) 391.
- [38] S.M. Scarott, S. Watkin, J.R. Miles, and P.J. Sarre, *Mon. Not. R. Astron. Soc.* 252 (1991) 229.
- [39] J.R. Miles, Ph.D. Thesis (1994).
- [40] B. Ehrenberg and F.M. Johnson, *Spectrochim. Acta*, 46A, 10 (1990) 1521-1532.
- [41] F.M. Johnson, *Ann. N. Y. Acad. of Sci.* 187 (1972) 186-206.
- [42] F.M. Johnson, *Mem. Soc. Roy. Scien. Liege* 6, III (1972) 391-407.
- [43] J.E. Falk, *Porphyryns and Metalloporphyryns vol. 2*, Elsevier Publishing Company, New York, 1964.
- [44] K.M. Smith (Ed.), *Porphyryns and Metalloporphyryns*, Elsevier Publishing Company, New York, 1975.
- [45] D. Dolphin (Ed.), *The Porphyrins*, Academic Press, New York, 1978.
- [46] A. Andreoni, and R. Cubeddu (Eds.), *Porphyryns in Tumor Phototherapy*, Plenum Press, New York, 1984.
- [47] F.M. Johnson and J.F. Becker in: A. Andreoni and R. Cubeddu (Eds.), *Porphyryns in Tumor Photo Therapy*, Plenum Press, New York, 1984, pp.101-105.
- [48] F.M. Johnson, B. Ehrenerg and E. Gross, *SPIE Photodynamic Therapy: Mechanisms* 1203 (1990) 11.
- [49] A. Lavi, F.M. Johnson, B. Ehrenberg *Chem. Phys. Lett.* 331 (1994) 144-150.
- [50] J. Moan, *Photochem. Photobiol.* 43 (1986) 681-690.
- [51] T.J. Dougherty, S.L. Marcus, *Eur. J. Cancer.* 28A (1992) 1734-1742.
- [52] J.C. Goedheer, and J.P.J. Siero, *Photochem. Photobiol.* 6 (1967) 509.
- [53] J.C. Goedheer, *Photochem. Photobiol.* 6 (1967) 521.
- [54] F.M. Johnson, *Chemical Identification of Interstellar Dust*, *Astron J.* 72 (1967) 305.
- [55] F.M. Johnson in: R.D. Enzman (Ed.), *Use of Space Systems for Planetary Geology and Geophysics*, AAS Science and Technology Series, vol. 17, Am. Astronautical Soc., Tarzana, CA 1967 pp. 51.
- [56] F.M. Johnson in: J.M. Greenberg and T.P. Roark, (Eds.) *Interstellar Grains*, NASA SP-140, 1967, p. 229-240.
- [57] F.M. Johnson, *Spectroscopic Studies of Interstellar Grains*, NASA CR-1667

- (1970).
- [58] F.M. Johnson, D.T. Bailey, P.A. Wegner in: J.M. Greenberg and H.C. Van de Hulst (Eds.), *Interstellar Dust and Related Topics IAU, Symp. 52, 1973*, pp. 317-321.
- [59] F.M. Johnson and D. Rosenthal, *Bull. Am. Astron. Soc.* 5, 4 (1973) 422.
- [60] F.M. Johnson, *Bull. Am. Astron. Soc.* 3 (1977) 429.
- [61] F.M. Johnson, *Voyage Into Astronomy*, Kendall Hunt Publishing Company, Dubuque, Iowa, 1977, pp. 192-208.
- [62] F.M. Johnson, *Bull. Am. Astron. Soc.* 23, 2 (1991) 933.
- [63] F.M. Johnson, *Bull. Am. Astron. Soc.* 25, 2 (1993) 820-821.
- [64] J. Linstead, *J. Chem. Soc.* 105 (1953) 2873.
- [65] R.B.M. Koehorst et al., *J. Chem. Soc., Perkin II* (1981) 1005.
- [66] F.M. Johnson, *Color Centers in Alkali Hydrides. Radiation Laboratory Progress Report*, Columbia University (1955) 30.
- [67] R.L. Hibbins, J.R. Miles, P.J. Sarre, and G.H. Herbig in: A.G.G.M. Tielens (Ed.), *NASA Conference Publication*, 10144, 1994.
- [68] A.M. Merle, M. Lamotte, S. Risemberg, C. Hauw, J. Gaultier, and J. Grivet, *J. Chem. Phys.* 22 (1977) 207.
- [69] A.M. Merle, W.M. Pitts, and M.A. El-Sayed, *Chem. Phys. Lett.* 54 (1978) 211-216.
- [70] A. M. Merle, M. F. Nicol, and M.A. El-Sayed, *Chem. Phys. Lett.* 59 (1978) 386.
- [71] E.C.M. Keilman and G.W. Canters, *Spectrochim. Acta, Part A*, 35 (1979) 1089-1099.
- [72] N.I. Morrell, N.R. Walborn, E.L. Fitzpatrick, *Pub. Astron. Soc. Pac.* 103 (1991) 341-346.
- [73] S.H. Fitch, C. P. Hayman, and D.H. Levy, *J. Chem. Phys.* 73 (1980) 1064.
- [74] U. Even, J. Magen, and J. Jortner, *J. Chem. Phys.* 77 (1982) 4384.
- [75] P.H. Siegel 2002, Private communication.
- [76] T.P. Snow, D. Zukowski and P. Massey, *Astrophys. J.* 578 (2002) 877.
- [77] T. Stecher, *Astrophys. J.* 142 (1964) 1681.
- [78] M. J. Seaton, *Mon. Not. R. Astron. Soc.* 187 (1979) 73.
- [79] B.D. Savage and J.S. Mathis, *Ann. Rev. Astr. Ap.* 17 (1979) 73.
- [80] A.N. Witt, R.C. Bohlin and T.P. Stecher, *Astrophys. J.* 279 (1984) 698.
- [81] J.A. Cardelli. and B.D. Savage, *Astrophys. J.* 325 (1988) 864.
- [82] J.A. Cardelli, C. Clayton and J.S. Mathis, *Astrophys. J.* 345 (1988) 245.
- [83] E.L. Fitzpatrick, D. Massa, *Astrophys. J.* 307 (1986) 286-294;
Astrophys. J. 328, 734.
- [84] C.G. Seab, T.P. Snow and C.L. Joseph, *Astrophys. J.* 246 (1981) 788.
- [85] T.P. Snow and C.G. Seab, *Astrophys. J.* 382 (1991) 189-192.
- [86] M.A. El-Sayed, M. Kasha, Y. Tanaka, *J. Chem. Phys.* 34 (1961) 334;
J. Chem. Phys. 36 (1962) 552.
- [87] H. Van Winckel, M. Cohen and T.R. Gull, *Astron. Astrophys.* 390 (2002) 147-154.
- [88] C.G. Seab, 1993, Private communication.
- [89] S.J. Fossey, *Nature* 353 (1991) 393.
- [90] P.J. Sarre, J.R. Miles and S.M. Scarrott, *Science* 269 (1995) 674-676.
- [91] S.M. Scarrott, S. Watkin, J.R. Miles and P.J. Sarre, *Mon. Not. R. Astron. Soc.*

- 255 (1992) 11.
- [92] R.J. Glinski and C.M. Anderson, *Mon. Not. R. Astron. Soc.* 332 (2002) 17.
- [93] G.D.Schmidt, M. Cohen, and B. Margon, *Astrophys. J.* 239 (1980) L133-L138.
- [94] M. Gouterman, *J. Mol. Spectrosc.* 6 (1961) 138; D. Dolphin (Ed.), *The Porphyrins*, Vol. III, Academic Press, London, 1978, pp.1-166.
- [95] X.-Y. Li, LA. Lipscomb, C.K. Chang and N.T. Yu in: W. Kiefer et.al (Eds.), *Proc. Intl. Conf. Raman Spectroscopy* 13 Wiley Publ., 1992, p. 326.
- [96] T.G. Spiro, R.S. Czernuszewicz and X.-Y. Li, *Coord. Chem. Rev.* 100 (1990) 541.
- [97] X.-Y. Li, 1993, Private communication.
- [98] F.K. Richtmyer and E.H. Kennard, *Introduction to Modern Physics*, McGraw-Hill Book Company, Inc., New York, 1947.
- [99] J. Krelowski and C. Sneden, *Publ. Astron. Soc. Pac.* 105 (1993) 1141-1149.
- [100] K. Lumme and J. Rahola, *Astrophys. J.* 425 (1994) 653-667.
- [101] G. Herzberg, *Mem. R. Soc. Liege Ser.15A* (1955) 291-331.
- [102] G. Herzberg in: H. van Woerden (Ed.), *IAU Symp. 31*, Academic Press, London, 1967, p. 91.
- [103] G. Herzberg, *Roy. Astron. Soc. Canada* 82 (1977) 115.
- [104] G.W. Hodgson in: F.M. Johnson (Ed.), *Interstellar Molecules and Cosmochemistry*, *Ann. N.Y. Academy of Science*, 194, 1972, p. 86-97.
- [105] G.W. Hodgson, *Ann. N.Y. Acad. of Science* 206 (1973) 670-684.
- [106] G.W. Hodgson and B.L. Baker, *Nature* 216, 5510 (1967) 29-32.
- [107] G.W. Hodgson and B.L. Baker, *Geochimica et Cosmochimica Acta* 33 (1969) 943-958.
- [108] D.J. Casagrande and G.W. Hodgson, *Geochim. Cosmochim. Acta*, 38 (1974) 1745-1758.
- [109] J.S. Mathis, 1994, Private communication.
- [110] W.M. Irvine, M. Ohishi, N. Kaifu, *Icarus* 91 (1991) 2-6.
- [111] A. Cox (Ed.). *Allen's Astrophysical Quantities*, 4th Edn., 1999, pp. 135-136.
- [112] K. Kawaguchi, E. Kagi, T. Hirano, S. Takano, S. Saito, *Astrophys. J.* 406 (1993) L39-L42.
- [113] F.M. Johnson, *Mem. Soc. Roy. Scien. Liege* 6, III (1972) 609-627.
- [114] F.M. Johnson, *Voyage into Astronomy*, Kendall Hunt Publishing Company, Dubuque, Iowa, 1977, p.p. 268-282, 289-294.
- [115] P.R. Shapiro and K.A. Holcomb *Astrophys J.*, 310 (1986) 872-888.
- [116] E.M. Purcell and P.R. Shapiro, *Astrophys. J.* 214 (1977) 92-105.

LIST OF TABLES

Tables 1a. to 1i. Vibrational Frequencies of Tetrabenzoporphyrins Plus (MgP) Mg-porphine.

Table 1a- columns 1 & 2 contain data derived from spectra originally taken for this project by Drs.D.Brumbaugh and U. Even respectively.

Tables 1b-1i contain commissioned LIF data of MgTBP by Dr.Brumbaugh column (1) and Raman data (column 12) supplied by Dr. Markwort

Table 2. Lab Spectra vs. DIBs

Table 2- Column 1 lists probable and definitive DIBS taken from the published literature. [2] is from Dr. George Herbig, designated by "H", the rest is from a survey paper [37]. Columns 2 and 5 list the totality of all of the author's quasiline Shpolskii lab data. Column 4 lists the number of individual measurements taken for each of the data points. The author's data in column 5 is the average value of the total number (n) of measurements for each spectral data point.

Table 3 Shpolskii lab spectra of MgTBP at 77K in the blue spectral region (including the Soret band) and assigned vibronic transitions. Note: confirmation of the S_2 splitting. The author's data is listed in column 3. Column 5 is the same data converted to wave-numbers. Columns 6 and 7 list the vibrational frequencies corresponding to each of the vibronic transitions. These vibrational frequencies are consistent with the derived frequencies shown in Table 1. A typical measured lab Soret band of MgTBP at 4428.2 Å, shown in Figure 3, is superimposed with astronomical data from [72].

Tables 4a to 4c. Shpolskii lab spectra of MgTBP at 77K and its interpretation, involving sites and tentative assignments of vibrational frequencies associated with the vibronic transitions.

Table 5- Lists reported astronomical data and probable DIBS in the blue spectral region from the sources indicated below. Columns 4 and 5 list vibrational frequencies for each of the corresponding vibronic transitions. Vibrational frequencies are consistent with frequencies listed in Table 1, and hence confirm the MgTBP designation.

Table 6. DIBs and their corresponding vibronic transitions for HD29647.

This is the interpretation of astronomical data based on the work of [7] and vibrational frequencies from Table 1.

Table 7. Potential sites and the corresponding frequencies for the indicated DIBs.

This table is an abbreviated extension of Table 4, listing potential "sites" and the corresponding frequencies (from Tables 1e and 1f) associated with the vibronic transitions for DIBS 5797.11 and 5849.78 Å.

Table 8. The blue fluorescence spectra of HD44179, (measured from Fig. 1 Schmidt, et al. [93]) and its interpretation. The electronic origin is at 25344.7 cm^{-1} . Column three lists the assigned vibrational frequencies corresponding to each of the vibronic transitions.

Table 1a. Vibrational Frequencies of Tetrabenzoporphyrins plus Magnesium Porphyrin (MgP).

MgTBP						CdTBP	ZnTBP		MgP	H ₂ TBP	MgTBP	
		[7]		Johnson		[7]	[74]	[13]	[26]	Johnson		
Bare		Matrix, n-Octane 4 K		Matrix, Quasiline 77 K		FTIR	4 K	Bare	Matrix	Matrix, 4 K	Matrix, 77 K	Raman
S_1	S_2	S_1	S_2	S_0	S_2	S_0	(S)	(S)	(S)	(S)	(S)	S_0
1	2	3	4	5	6	7	8	9	10	11	12	13
10	11		10.5	11		11.3 microwave		10 a				
	18	17	18	18				18 a	18	17		
20			20	20	21					21		
			22.5	22								
24			25	25					24			
	26		27	27	28					27		
	33		33							35		
40	40		40	41	42							
44	44		44	44			44			43		
	61	62	61.5	62			62			62		
	74		73	73								
77	78		77	77					80			
	85		85	85	85					87		
94	92	90	92	92, 93	93	Start of FTIR data					90	
	100		99	98							100	
110	110	113	109/111	111		111						
118	117	119	117	116, 118								
128	126		126	125				124	123			
131				131		129			131			

146			146	146		143						
	149		150	152		152	150	148				
156	155		156	154, 156	156							
		159, 162	161	159, 161		161						
	168		167									
172		172, 174	172	173, <175>								
172		172, 174	172	173, <175>								
			180	180		181		179			182	
	187		186	185								
			189				189, 191			189	190	
	197	194	195	195, 197		195	197		197	193		
	210		209	210								
217			215	216							217	
	220	221	221	219, 221		220				220	220	
231			230	230					234	227	227	
238	238	239	vs 238	238			238	238		236		239
			242	242				242				
	244	244	vs 244	244					243			
247		248	246	247				248			247	
	End of data	257	257			255	256, 258	254				
		261	260	259			259	257				
			265			264			264			
			270			270						
		276	275	275								
			282	281				281				

		287	287	288		287		288				
			290									
		303	297	304				301				
312		311	311	311		311	309					

Columns 1 and 2 contain data derived from spectra originally taken for this project by Drs. D. Brumbaugh and U. Even, respectively.

Table 1b. Vibrational Frequencies of Tetrabenzoporphyrins plus Magnesium Porphyrin (MgP)

MgTBP						CdTBP	ZnTBP		H ₂ TBP	MgP	MgTBP
	[7]		Johnson			[7]	[74]	[13]	Johnson	[26]	
Bare	<i>n</i> -Octane 4 K		Quasiline 77 K		FTIR	4 K	Bare	Matrix	Matrix	4 K	Raman
<i>S</i> ₁	<i>S</i> ₁	<i>S</i> ₀	<i>S</i> ₀	<i>S</i> ₁	<i>S</i> ₀	<i>S</i> ₀	<i>S</i> ₁ , <i>S</i> ₂	(<i>S</i>)	(<i>S</i>)	(<i>S</i>)	<i>S</i> ₀
1	2	3	4	5	6	7	8	9	10	11	12
					334				328		330 w
	341		342				351				
	353				355		355			365	
	359		357, 360		363		362				
378			378		376		366				
386	383		383, 388				386	386			
393			392, 394		390					394	
401			400				398	397	402	401	
			442		422				431		
	460	462	461				456, 460		452		
					474		468				475
478	477	480	478, 481		480	477, 480	480	482			477, 480
			485					486			
488	489	487	489, 491				490				
505	504		502, 504	502	501		498	499	499, 503		
507	507		507	507	507						

514	519		518				515	512	517		
					521				522		
	539		539	538	532	538	540				
548	548		547, 549				548				
			552		550						551
557	558, 562		559	557			559				

Commissioned LIF data of MgTBP by Dr. Brumbaugh column (1) and Raman data (column 12) supplied by Drs. Markwort and N. Spingarn.

Table 1c Vibrational Frequencies of Tetrabenzoporphyrins plus Magnesium Porphyrin (MgP)

MgTBP						CdTBP	ZnTBP		H ₂ TBP	MgP	MgTBP	
	[7]		Johnson			Spingarn	[7]	[74]	[13]	Johnson	[26]	
Bare	<i>n</i> -Octane 4 K		Quasiline 77 K		FTIR	Reflection 300 K	4 K	Bare	Matrix	Matrix	4 K	Raman
<i>S</i> ₁	<i>S</i> ₁	<i>S</i> ₀	<i>S</i> ₀	<i>S</i> ₁	<i>S</i> ₀	<i>S</i> ₀	<i>S</i> ₀	<i>S</i> ₁ , <i>S</i> ₂	(<i>S</i>)	(<i>S</i>)	(<i>S</i>)	<i>S</i> ₀
1	2	3	4	5	6	7	8	9	10	11	12	13
566	569		569	568	571				568	566		
577	578		580		580		578	577	575			580,581
		582	583, 585		584							583
591	591/592	593	593					589		588		
			595 s	593	594							
599	599.5		599	597	600		602		601	598		598 w
	615		616	615	615							618
619	621	625	626	628	625							
629	629	629			633							
635	639	637	636, 639	639	640 w				633			637
	646		646	643, 646	650		651					
	659	659	659	659	660					660		
675	678	679, 674	675	676	679 w		676			674		
689							686					
692	691							691		693		
695		697	695	695 s	695 s			698		697		696 s
701		704	702	702 s	705			704	703	701		701
710	709	707	708	706	708	707	708		710		708	
713		712	711, 712	711							713	

		722	721, 725							720	724	
728		727	727					729		726	730	
733		732	732, 734	731							734	733, 734
736		737	737	737		738						737
739	739	739	742		741			739	740		741	739
751		752	751			754			745			
760		758			757							
763		762	763		764			764				760sh

Commissioned LIF data of MgTBP by Dr. Brumbaugh column (1) and Raman data (column 13) supplied by Drs. Markwort and N. Spingarn.

Table 1d Vibrational Frequencies of Tetrabenzoporphyrins plus Magnesium Porphyrin (MgP)

MgTBP						CdTBP	ZnTBP		H ₂ TBP	MgP	MgTBP	
	[7]		Johnson			Spingarn	[7]	[74]	[13]	Johnson	[26]	
Bare	<i>n</i> -Octane 4 K		Quasiline 77 K		FTIR	Reflection 300 K	4 K	Bare	Matrix	Matrix	4 K	Raman
<i>S_l</i>	<i>S_l</i>	<i>S_o</i>	<i>S_o</i>	<i>S_l</i>	<i>S_o</i>	<i>S_o</i>	<i>S_o</i>	<i>S_l, S₂</i>	(<i>S</i>)	(<i>S</i>)	(<i>S</i>)	<i>S_o</i>
1	2	3	4	5	6	7	8	9	10	11	12	13
769		769 vs	768, 770	767								
776		774	774	773								
783	783							784			782	784
786		788	787	787 _s						786		
792			794					792				
										798, 801	798	
818		818	819					816				818 _s
	–	821					820	820			821	820
824	825	826	824				825, 828	827	827		824	825
830	832	833	831		831	830	830			830	827	
835		–	836				–	–	–	–		
–	842	–	840				843	839		838	–	840
845		–	845				848	845				
850	851	851	851				851					852 _w
–	855	–	854				–					
–	863	864	865			865	862	861				
										870		
	887	886	885		889	887				893	888	

		895	895		891							899 w
		904	904	905 s							909	
914		916	913									918
											933	
932		934	936		937	940		935			937	937
954 w			955					957	958		957	950
972		974	971, 975	975	974 w						965	964
979			979									980
989 w				986 s							989	

Commissioned LIF data of MgTBP by Dr. Brumbaugh column (1) and Raman data (column 13) supplied by Drs. Markwort and N. Spingarn.

Table 1e Vibrational Frequencies of Tetrabenzoporphyrins plus Magnesium Porphyrin (MgP)

MgTBP							CdTBP	ZnTBP		H2TBP	MgP	MgTBP
	[7]		Johnson			Spingarn	[7]	[74]	[13]	Johnson	[26]	
Bare	n-Octane 4 K		Quasiline 77 K		FTIR	Reflection 300 K	4 K	Bare	Matrix	Matrix	4 K	Raman
S ₁	S ₁	S ₀	S ₀	S ₁	S ₀	S ₀	S ₀	S ₁ , S ₂	(S)	(S)	(S)	S ₀
1	2	3	4	5	6	7	8	9	10	11	12	13
998		995	997		1001						994	
											998	
	1007	1006	1007	1006			1008				1007	
			1011	1011						1010 IR	1011	1010
1019			1017, 1018		1015	1015	1015, 1018				1013	1018
1023												
1026		1026	1025									
1030			1029									
			1034					1032		1033		
	1037	1036	1037	1035, 1037	1036					1036		1035
	1043		1040		1040						1041	1043
		1056			1057	1052				1065	1057	
	1063	1060	1061								1060	1059
	1067						1070		1066	1070		
							1080		1074			
1079	1078		1080	1081								1080
	1093		1092				1093			1092	1091	1095

1099	1098		1097				1096			1098, 1101		
	1105	1106	1106	1105			1106					
1109			1110	1110			1110			1110		
1111	1111	1111	1112	1112	1111	1111	1113	1114		1112		
1116	1116		1116	1117	1119		1117				1116	1117, 1118
					1121			1121	1123			
	1127		1128									
1131	1131		1132	1133, 1136			1135					

Commissioned LIF data of MgTBP by Dr. Brumbaugh column (1) and Raman data (column 13) supplied by Drs. Markwort and N. Spingarn.

Table 1f. Vibrational Frequencies of Tetrabenzoporphyrins plus Magnesium Porphyrin (MgP)

MgTBP							CdTBP	ZnTBP		H ₂ TBP	MgP	MgTBP
	[7]		Johnson			Spingarn	[7]	[74]	[13]	Johnson	[26]	
Bare	n-Octane 4 K		Quasiline 77 K		FTIR	Reflection 300 K	4 K	Bare	Matrix	Matrix	4 K	Raman
S_I	S_I	S_O	S_O	S_I	S_O	S_O	S_O	S_I, S_2	(S)	(S)	(S)	S_O
1	2	3	4	5	6	7	8	9	10	11	12	13
1153			1153				1150	1151				1151
			1156				1155			1155		1154
	1158	1158	1158	1158	1157			1160	1159		1159	
	1162			1164							1164	
1167							1167					
		1170		1169			1169					
1175	1173		1174	1172			1173			1174		
	1179	1184		1184			1179	1181		1183	1178	1179
1185	1186	1187	1187					1187		1187	1189	
	1187		1189									
	1190 w					1191						
1195	1192 w		1195	1195			1196					1196
	1200		1200	1200	1202							
1212	1212	1214	1210		1214		1206	1208		1209		
1219	1219	1219	1218, 1220	1220	1217					1215	1219	
1221			1223									
			1226									1225, 1226
	1229		1231	1231			1235			1234	1235	
1237	1238		1237		1236	1236			1238			1240

	1249	1249	1252	1251					1251			
	1260	1258	1257, 1260				1256				1262	1258 w
1264												1264 w
1266	1267		1267 w	1267			1268					
1271	1273	1271	1272	1270	1271 w					1271		
1276	1275	1275	1277				1274	1274		1274		
					1291			1280				1291 w
1297	1297	1299	1296	1298	1296	1294	1299	1293		1299		

Commissioned LIF data of MgTBP by Dr. Brumbaugh column (1) and Raman data (column 13) supplied by Drs. Markwort and N. Spingarn.

Table 1g. Vibrational Frequencies of Tetrabenzoporphyrins plus Magnesium Porphyrin (MgP)

MgTBP							CdTBP	ZnTBP		H ₂ TBP	MgP	MgTBP
	[7]		Johnson			Spingarn	[7]	[74]	[13]	Johnson	[26]	
Bare	<i>n</i> -Octane 4 K		Quasiline 77 K		FTIR	Reflection 300 K	4 K	Bare	Matrix	Matrix	4 K	Raman
<i>S</i> ₁	<i>S</i> ₁	<i>S</i> ₀	<i>S</i> ₀	<i>S</i> ₁	<i>S</i> ₀	<i>S</i> ₀	<i>S</i> ₀	<i>S</i> ₁ , <i>S</i> ₂	(S)	(S)	(S)	<i>S</i> ₀
1	2	3	4	5	6	7	8	9	10	11	12	13
1308	1309		1309				1310			1307	1305	1310
1313	1314	1315	1313, 1316						1315			
1320			1321		1321		1322				1319	
1323	1324							1323	1324		1324	1323
1325	1327		1327?	1329	1329	1329						1330
										1331		
		1336	1336	1334			1335		1334			
1337		1338	1338	1339	1338		1337			1337		

End of data									1341			
	1342, 1345	1345	1342, 1347		1348 w		1346			1346		
	1353	1353	1352		1356 w		1353	1350	1351	1356		
				1365	1362						1363	
	1370	1368	1367, 1370								1369	1367, 1370
	1374		1374	1375	1373		1373					
	1380	1383					1382			1380		1378
	1387	1387	1388	1389	1387		1391	1388				
	1396		1396, 1398	1394	1396					1397	1397	1394
	1402		1400	1401								
		1417			1418	1413	1412					1409 w
	1420		1420	1420						1420		
	1426	1423		1425	1427 w					1426		
	1435	1435	1434, 1436	1435, 1438	1439					1433	1443	1436
	1451	1452	1450	1451 s	1446						1457	
				1456	1458	1454			1456			
			1465	1466	1466			1466		1468		1464 w
		1473	1473	1473	1474	1476				1474		1475 w

Commissioned LIF data of MgTBP by Dr. Brumbaugh column (1) and Raman data (column 13) supplied by Drs. Markwort and N. Spingarn.

Table 1h. Vibrational Frequencies of Tetrabenzoporphyrins plus Magnesium Porphyrin (MgP)

MgTBP						CdTBP	ZnTBP		H ₂ TBP	MgP	MgTBP	
	[7]		Johnson		Spingarn	[7]	[74]	[13]	Johnson	[26]		
Bare	<i>n</i> -Octane 4 K		Quasiline 77 K		FTIR	Reflection (300 K)	4 K	Bare	Matrix	Matrix	4 K	Raman
<i>S</i> ₁	<i>S</i> ₁	<i>S</i> ₀	<i>S</i> ₀	<i>S</i> ₁	<i>S</i> ₀	<i>S</i> ₀	<i>S</i> ₀	<i>S</i> ₁ , <i>S</i> ₂	(S)	(S)	(S)	<i>S</i> ₀
1	2	3	4	5	6	7	8	9	10	11	12	13
	1481		1482		1481							
					1489						1487	1490 w
					1496		1495				1496	1496
		1502		1502			End of data				1500	1502
			1509	1508	1507				1510	1502	1508	1508
			1518		1518			1516		1521		1515
		1536	1535	1534 _s	1533	1536		1528		1532		
				1540	1541			End of data		1538, 1540		
		1551	1549		1550					1550	1546	1549, 1555, 1552
				1557	1559						1563	1561
		1566	1568		1568				1570		1566, 1570	1568
		1585	1588	1588	1585							1586
			1600	1598	1593					1601	1601	1598, 1596
						1606					1609	
		1615	1613		1616					1617	1611	

		1618	1618								1619	1620
		End of data	1626	1624	1626				1626	1624, 1627		
			1636	1634	1636				End of data	End of data		
			1642, 1644		1645						1647	
			1652		1653						End of data	
			1663, 1666	1660	1663							1669
			1674		1676							
			1683		1684							1687
			1698	1696	1697							

Commissioned LIF data of MgTBP by Dr. Brumbaugh column (1) and Raman data (column 13) supplied by Drs. Markwort and N. Spingarn.

Table 1i. Vibrational Frequencies of Tetrabenzoporphyrins plus Magnesium Porphyrin (MgP)

MgTBP						CdTBP	ZnTBP		H ₂ TBP	MgP	MgTBP	
	[7]		Johnson			Spingarn	[7]	[74]	[13]	Johnson	[26]	
Bare	n-Octane 4 K		Quasiline 77 K		FTIR	Reflection 300 K	4 K	Bare	Matrix	Matrix	4 K	Raman
S ₁	S ₁	S ₀	S ₀	S ₁	S ₀	S ₀	S ₀	S ₁ , S ₂	(S)	(S)	(S)	S ₀
1	2	3	4	5	6	7	8	9	10	11	12	13
			1719		1717							1722 s
			1728									
			1734	1734 s	1734							
			1740		1745							1739 w
			1750		1749							1750
			1760		1762							1765 s
			1769, 1775		1772							
					1782							1779
					1792							End of data
			1801, 1805		1802							
			1810		1811							
			1816		1828							
			1847		1845							
					1859							
			1872		1869							
					1946							

						3050						

Commissioned LIF data of MgTBP by Dr. Brumbaugh column (1) and Raman data (column 13) supplied by Drs. Markwort and N. Spingarn.

Table 2. Lab Spectra vs. DIBs

Probable DIBs	Lab Wide	Notes	n	Lab Å
4131			6	4130.0
4169.9			5	4170.5
4175		H	4	4175.0
4186		b	5	4184.9
4187.5		b	2	4187.7
4268			2	4268.0
4277			6	4276.5
4283		vs	5	4282.9
4286			1	4287.5
4301			2	4301.5
4305			2	4304.5
4308			2	4307.8
4314			4	4315.1
4320		b	3	4320.4
4326			6	4325.5
4329			3	4329.5
4333			1	4334.1
4350			1	4351
4357			1	4357.5
4426			1	4424.8
4428		H/Soret	11	4428.2
4437.5			2	4437.1
4440			1	4438.8
4444			4	4444.5
4447.5			2	4447.2
4453			3	4454.1
4512.8			1	4512.3
4522.5			1	4521.6
4528 br			3	4527
4550			1	4551.2
4581 br			1	4579.8
4614			2	4613.9
4621 br			1	4622.6
4631			4	4631.5
4635.8			1	4636.2
4642.8			1	4642.6
4682.5?			1	4681.3
4710.5?			1	4710.4
5264.8			2	5265.5
5711.5			1	5712.4
			3	5755.8

Probable DIBs	Lab Wide	Notes	n	Lab Å
5762.5			3	5761.8
5768			1	5767.5
5797 _{vs}		H	5	5798
5813.5			4	5813.8
5844		H	1	5843.4
			1	5863.7
5872			3	5872.1
5899			8	5898
6016			1	6017.1
6030			4	6032.4
6038			3	6039
6071			1	6069.8
6078			2	6078
6247.5			1	6248
			1	6254
			1	6258.8
			1	6264
6270		H	4	6269.4
6272			1	6273.5
6279			7	6278.2
6281			5	6282.0
6284		H	4	6284.0
6288			4	6288.5
6290		absorption	6	6291
			5	6294.1
			10	6297.3
			4	6301.6
6307		H	2	6306.7
6314		H	18	6314.6
6318		H	6	6318.3
			7	6322.9
			10	6328.4
6331			1	6331.1
6335			1	6333
6345	6345		6	6345.7
6354	6354	H	1	
6357? _{em}			7	6355.9
6362	6361	H	1	
6365	6365		5	6364.7
6367		H	4	6367.3
	6370		2	6373.7
6376		H	1	6377

Probable DIBs	Lab Wide	Notes	n	Lab Å
6379		H	1	6379
6383?			1	6381
6397		H	1	6397
6400			1	6398.8
6410			1	6409.5
6432.8			1	6431.7
6439.5		H	2	6441.2
6445.3		H	3	6445.8
6449.3		H	1	6451.0
6456			1	6455.5
6466.8?			5	6465.7
6474			9	6476.9
6482			8	6481.6
6489			5	6488.7
6492			1	6491.5
6495 wide			10	s6494.9
6502			2	6502.8
6507	6508		2	6508.8
6509			9	6511.5
			12	6513
	6515		9	6514.5
			2	6530.5
			5	6533.0
	6538		5	6536.7
			2	6552.4
			4	6562.6
			1	6568.7
			3	6574.0
			1	6576
6578.5			4	s6578.2
6583			8	6582.0
			1	6587.0
			1	6590
			2	6591.5
6597			5	6595.5
6600			1	6600
6603 w			8	6602.9
	6604		2	6605.4
6609?	6608		2	6609.2
6611			2	6611.3
6614			2	6614.6
			2	6618.0

Probable DIBs	Lab Wide	Notes	n	Lab Å
			9	6620.7
6622.5	6621		2	6623.5
6627	6627		4	6627.9
6633			1	6632.6
6635.3			3	6635.1
6638 w			2	6638.5
6642			1	6640.0
6649	wide		4	6647.6
			2	6650.6
6654			3	6654.4
6657			3	6656.3
			4	6658.4
6660.6		H	1	6662.6
6672			2	6672.7
			1	6677
			1	6680.2
6689.4			3	6690.2
6694.5			4	6694.5
6704.2			1	6705
6740.8		H	1	6740
6743.5			1	6744
6746			2	s6747.3
6750.5			1	6749
6752.7			1	6752.6
6756			2	6755.3
6758			1	6758
6775			1	6774.9
6792.4		H	1	6790.7
6795.2		H	1	6794.6
6809.3		H	3	6808.6
6811.1	wide	H	3	6811.0
6823.3		H	1	6824.2
6832.8		H	1	6832.2
6847.6		H	4	s6848.3
6852.5		H	3	s6853.3
			1	6865.1
			1	6882.2
			3	6889.5
			3	s6892.6
	6906		2	6908.2
6944.5	6931	H	2	6944.6
			1	6970.9

Probable DIBs	Lab Wide	Notes	n	Lab Å
6993		H	2	6993.1
7023.3			1	7022.9
7027.4			2	7027.5
7037	wide		1	7038
7050.2	wide		1	7050.2
He			3	7065.8
v7068.2			2	7068.0
7069.5			1	7070.3
7075			1	7075.4
7088			1	7088
7282.3			1	7283.4

n= number of measurements

H= Herbig designated DIBs

br= broad

v.s.= very sharp

s= strong

w= weak

Column 1 lists probable and definitive DIBs taken from the published literature. Source for Herbig data, designated by “H” is found in reference [2]. The rest is from a survey paper, see [37]. Columns 2 and 5 list the totality of all the author’s quasiline Shpolskii lab data. Column 4 list the number of individual measurements taken for each of the data points. The author’s data in column 5 is the average value of the total number (n) of the measurements for each spectral data point.

Table 3 Author's Shpolskii lab spectra of MgTBP at 77K in the blue spectral region (including the Soret band) and assigned vibronic transitions. Note: confirmation of the S₂ splitting.

Notes	n	Å	m.e Å	1/λ (cm-1)	Origins		Notes
					22444 S _{2x} (cm-1)	22479 S _{2y} (cm-1)	
	6	4130.0	0.3	24213	1769	1734	
	5	4170.5	0.4	23978	1534		
	4	4175.0	0.4	23952	1508	1473	
b	5	4184.9	0.5	23895	1451	1416	
b	2	4187.7	1	23879	1435	1400	
	2	4268.0	0.7	23430	986		
	6	4276.5	0.3	23384		905*	↑35 cm-1
vs	5	4282.9	0.3	23349	905*		↓
	1	4287.5	1	23324		845	
	2	4301.5	0.9	23248		769*	↑
	2	4304.5	0.3	23231	787	752	34cm-1
	2	4307.8	1	23214	770*	735	↓
	4	4315.1	0.6	23174		695	
b	3	4320.4	0.6	23146	702		
	6	4325.5	0.5	23119	675	640	
	3	4329.5	0.9	23097		618	
	1	4334.1	1	23073	629	594	
	1	4351	1	22983	539	504*	↑34 cm-1
	1	4357.5	1	22949	505*		↓
	1	4424.8	1	22600	156		
Soret	11	4428.2	0.4	22583	<139>		
	2	4437.1	0.3	22537	93		
	1	4438.8	1	22529	85		
	4	4444.5	0.3	22500		21	
	2	4447.2	1	22486	42		
	3	4454.1	1	22451		28	

n= number of measurements

b= broad

vs= very sharp

Table 4a Author's Shpolskii lab spectra of MgTBP at 77K and its interpretation involving sites and tentative assignments of vibrational frequencies associated with the vibronic transitions.

		MgTBP Fluorescence at 77K		Site I		Site II		Site III		Site IV		Site V		MgTBP Absorption lines At 77K	
D I B S	n	Narrow Lines A	cm ⁻¹	15913	15949	15882	15918	15944	15980	15872	15908	15810	15846	n	
				x	y	x	y	x	y	x	y	x	y		
				cm ⁻¹											
		6248	16005	-92		-123	-87	-61	-25	-133	-97	-195	-159		
		6254	15990	-77	-41	-108	-72		-10	-118	-82	-180	-144		
	1	6258.8	15977						0-0						
		6264	15964					-20		-92		-154	-118		
*	4	6269.4	15950		0 - 0					-78	-42			0	(6270.4) inferred
	1	6273.5	15940	-27	9			0-0	40		-32	-130	-94	2	6273.2
	7	6278.2	15928		21						-20	-118	-82	10	6277.4 mean
	5	6282.0	15918				0-0#	26	62		-10	-108	-72	5	6282.1
*	4	6284.0	15913	0-0										5	6284.4
	4	6288.5	15902	11				42	78						
			15896						84	-24		-86		6	6291
	5	6294.1	15888	25	61				92		20	-78	-42	5	6295.1
	10	6297.3	15879	34		0-0	39		101		29		-33	8	6298.9
	4	6301.6	15869	44					111	0-0	39				
			15864		85	18			116		44		-18	6	6303.5
*	2	6306.7	15856	57	93	26	62#						-10		
			15848										0-0	4	6309.8
*	18	6314.6	15836	76.7	112.7	45.7	81.7	107.7	143.7	35.7	71.7	-26.3	9.7		End of Absorption Data

Correlates with Ref. [11]

Table 4b Author's Shpolskii lab spectra of MgTBP at 77K and its interpretation involving sites and tentative assignments of vibrational frequencies associated with the vibronic transitions.

D I B s	77K MgTBP Quasiline Spectra Fluorescent Lines					Site I	Site II	Site III	Site IV	Site V	Sevchenko* Fluorescence Quasilines [11]					
	n	Wide	Narrow	m.e.	cm ⁻¹	15913	15949	15882	15918	15944		15980	15872	15908	15810	15846
		Å	Å			x	y	x	y	x		y	x	y	x	y
*	6		6318.3	0.3	15827	86		55	91	117		45				
	3		6322.2		15817											
	7		6322.9	0.8	15815	98	134			129			93			
	1		6324.7		15811			71				61	97	0-0		
	3		6327.3		15805	108	144	77	113		175				41	
	10		6328.4	0.6	15802	111	147		116						44	
	3		6331.1		15795	118	154	87		149	185	77	113			
			6333		15790		159	92		154	190		118	20		
	6	6345	6345.7	0.5	15759	154	190		159	185	221	113	149		87	
*	1	6354			15738	175	211	144	180		242			72		
*	7		6355.9	0.6	15733	180	216	149	185		247		175	77	113	
*	1	6361			15721			161	197		259	151	187		125	
	5	6365	6364.7	0.8	15711		238	171				161	197	99		
*	4		6367.3	0.6	15705	208	244			239	275	167				
		6370			15699		250			245	281	173	209	111	147	
	2		6373.7		15689		260		229	255	291		219		157	
*	1		6377		15681	232			237							6377
*	1		6379		15676	237			242		304	196	232			
			6381		15672	241		210	246				236		174	
*	1		6397		15632	281			286	312		240	276			
	1		6398.8		15630	283			288			242		180	216	
					15615	298	334		303			257		195	231	6404

Table 4c. Author's Shpolskii lab spectra of MgTBP at 77K and its interpretation involving sites and tentative assignments of vibrational frequencies associated with the vibronic transitions.

D I B S	77K MgTBP Quasiline Spectra Fluorescent Lines				Site I		Site II		Site III		Site IV		Site V		Sevchenko* Fluorescence Quasilines [11]	
	n	Wide	Narrow		15913	15949	15882	15918	15944	15980	15872	15908	15810	15846		
		Å	Å	m.e.	x	y	x	y	x	y	x	y	x	y		
		cm ⁻¹		cm ⁻¹												
*	1		6790.7		14726	1187	1223	1156		1218						
*	1		6794.6		14718	1195	1231	1164	1200	1226		1154	1190	1092		
*	3		6808.6	0.6	14687	1226		1195	1231	1257		1185	1221		1159	
*	3	wide	6811.0	0.5	14682	1231	1267	1200	1236		1298	1190	1226	1128	1164	
*					14671		1278	1211		1273	1309	1201	1237		1175	6816
*	1		6824.2		14653	1260	1296	1229		1327	1219		1157	1193	End of Data	
*	1		6832.2		14636	1277	1313	1246		1308		1236	1272	1174	1210	
*	4		s6848.3	0.9	14602		1347	1280	1316			1270				
*	3		s6853.3	0.5	14592	1321		1290	1326	1352			1316	1218		
	1		6865.1		14566	1347	1383	1316	1352							
	1		6882.2		14530	1383	1419	1352	1388		1450	1342			1316	
	3		6889.5	0.6	14515	1398	1434	1367			1465			1295		
	3		s6892.6		14508			1374		1436	1472		1400			
	2	6906	6908.2	0.2	14476	1437	1473	1406				1396		1334	1370	
	2	6931	6944.6	1	14400		1549	1482	1518			1472				
	1		6970.9		14345	1568		1537		1599	1635			1465	1501	
*	2		6993.1	2	14300	1613		1582	1618	1644						

Table 5. Reported and probable DIBs in the blue spectral region. Columns 4 and 5 list vibrational frequencies for each of the corresponding vibronic transitions. Vibrational frequencies are consistent with the frequencies listed in Table 1, and hence confirm the MgTBP designation.

Reference	DIBs(Å)	DIBs cm ⁻¹	22,444 S _{2x} cm ⁻¹	22,479 S _{2y} cm ⁻¹	FWHM (Å)	EW	New DIB ? Y=yes
S	4381	22,826	382	----			Y
S	4394	22,758	---	278			Y
S	4401	22,722	278	---			Y
S	4407.5	22,688	244	209			Y
S	4413	22,660	216	181			Y
S	4417	22,640	196	161			Y
S	4420	22,624	180	145			?
M em.	4485	22,296	148	183			
H	4501.7	22,214	230	265	2.8	190	
M em.	4503	22,207	237	---			
M	4525.5	22,097	---	382			Y
M	4535	22,051	393	---			Y
J & D	4595	21,762	751, 615	787, 646	28		
J & D	4665.5	21,434	1010	---	4		
H	4726.4	21,158	---	1321	3.4	175	
J & D	4727	21,155	---	1324	4		
H	4760	21,008	1481,1451	1518,1420	25	700	
			1420,1380				
J & D	4761.7	21,001	---	1478			
H	4762.7	20,996	---	1483	3.1	160	

Key: S= T.P. Snow, et. al. 2002, *Astrophys. J.* 578 (2002) 877 [76]

H= G.H. Herbig, *Annu. Rev. Astrophys.* 33 (1995) 19 [2]

M= N.I. Morrell, N.R. Walborn, E.L. Fitzpatrick, *Astro. Soc. of the Pac.* 103 (1991) 341-346 [72]

J&D= P. Jenniskens, and F-X. Desert, *Astron. Astrophys. Suppl.* 106 (1994) 39 [37]

Table 6. DIBs and their corresponding vibronic transitions for HD29647. This is the interpretation of astronomical data based on the work of [7] and vibrational frequencies from Table 1.

P & C [7] (Å)	DIBs (Å)	DIBs (cm ⁻¹)	15,962 origin	15,992 origin
5779	5780.7	17,299	1,337	1308
	5782.1	17,295	1,333	
	5784.2	17,288.5	1326.5	1296
	5785	17,286.1	1324	1294
	5791.2	17,267.6		1275
	5792.4	17,264.0		1272
5794	5794 em	17,259	1297	1267
	5794.3 em	17,258	1296	1266
	5795.1 em	17,256	1294	1264
	5795.4	17255	1293	1263

Table 7. Abbreviated extension of Table 4, listing potential sites and the corresponding frequencies (from Tables 1e & 1f) associated with the indicated DIBs.

←----- SITES ----->											
DIBs	cm ⁻¹	15,913	15,949	15,882	15,918	15,944	15,980	15,872	15,908	15,810	15,846
5797.11	17,250	1338	---	1368	1333	---	1271	1375	1342	1437	1400
5849.78	17,095	1184	---	1212	---	1153	1116	1223	1187	---	1249

Table 8. The blue fluorescence spectra measured from Fig. 1 of HD44179 (Schmidt, et al. [93]) and its interpretation. The electronic origin is at 25344.7 cm⁻¹. Column three lists the assigned vibrational frequencies corresponding to each of the vibronic transitions.

RR Emission (Å)	RR Emission (cm ⁻¹)	$\Delta\nu$ (cm ⁻¹)
3713	26,932	1587.7
3752	26,652	1308
3779	26,462	1117
3800	26,316	972
3851.5	25,964	619
3884	25,746.6	402
3908	25,588	243
3945.6	25,344.7	0-0
3979	25,132	213
4009	24,944	401
4044	24,728	617
4077	24,528	817
4119	24,278	1067
4136	24,178	1166
4167	23,998	1347
4255	23,499	1846

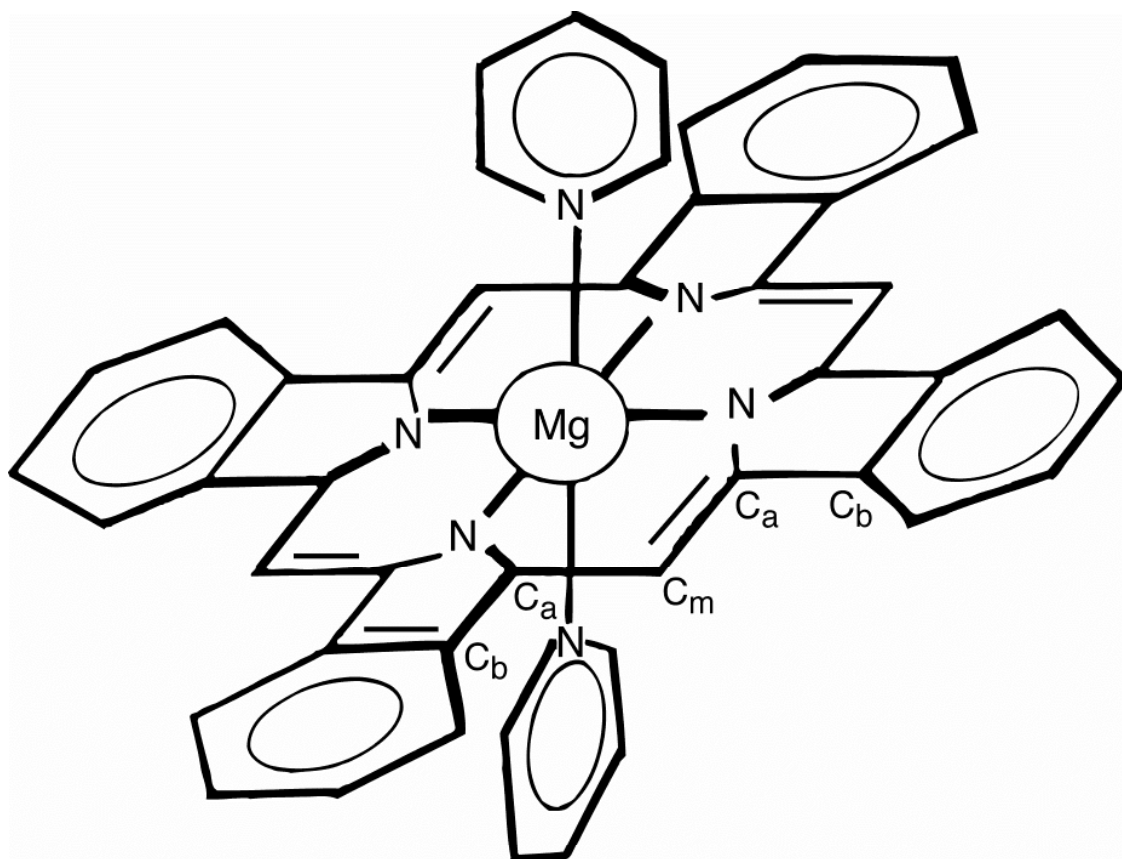


Figure 1. Dipyrrolyl magnesium tetrabenzoporphyrin ($\text{MgC}_{46}\text{H}_{30}\text{N}_6$)

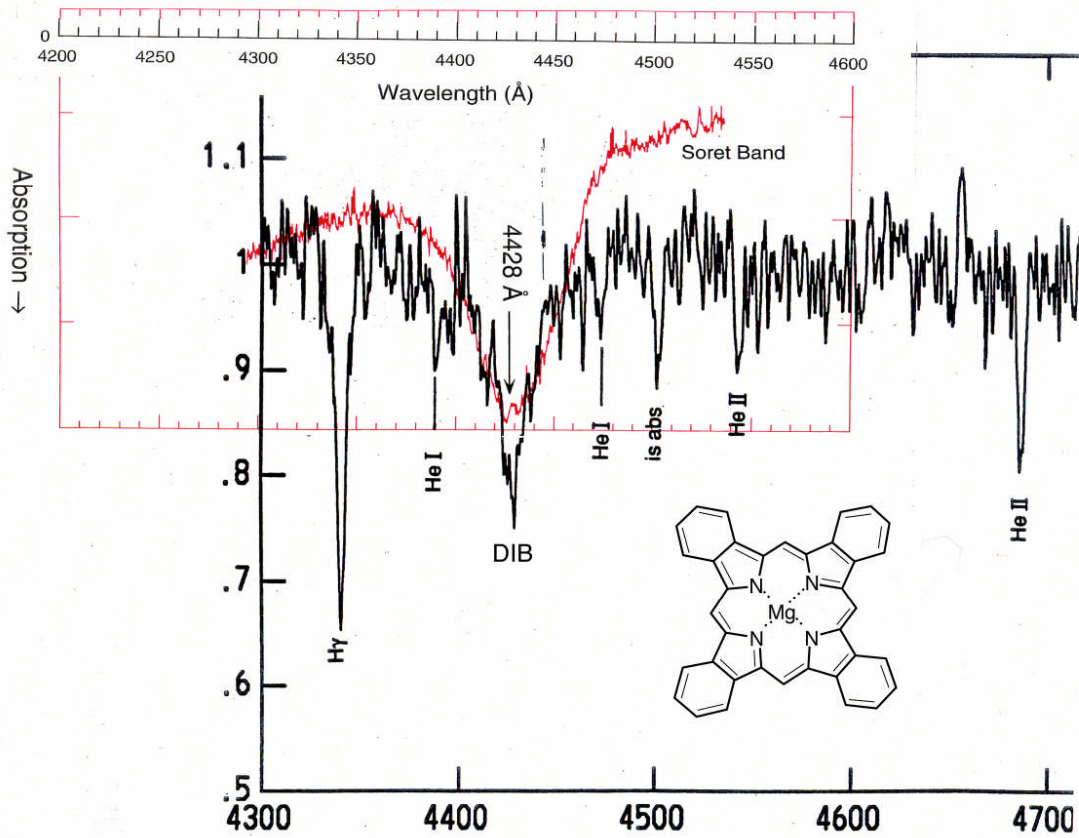


Figure 3. The superposition of MgTBP lab Soret band and the 4428Å DIB. Astronomical data from reference [72].

Superpositioned (red) lab Soret band is from author's data.

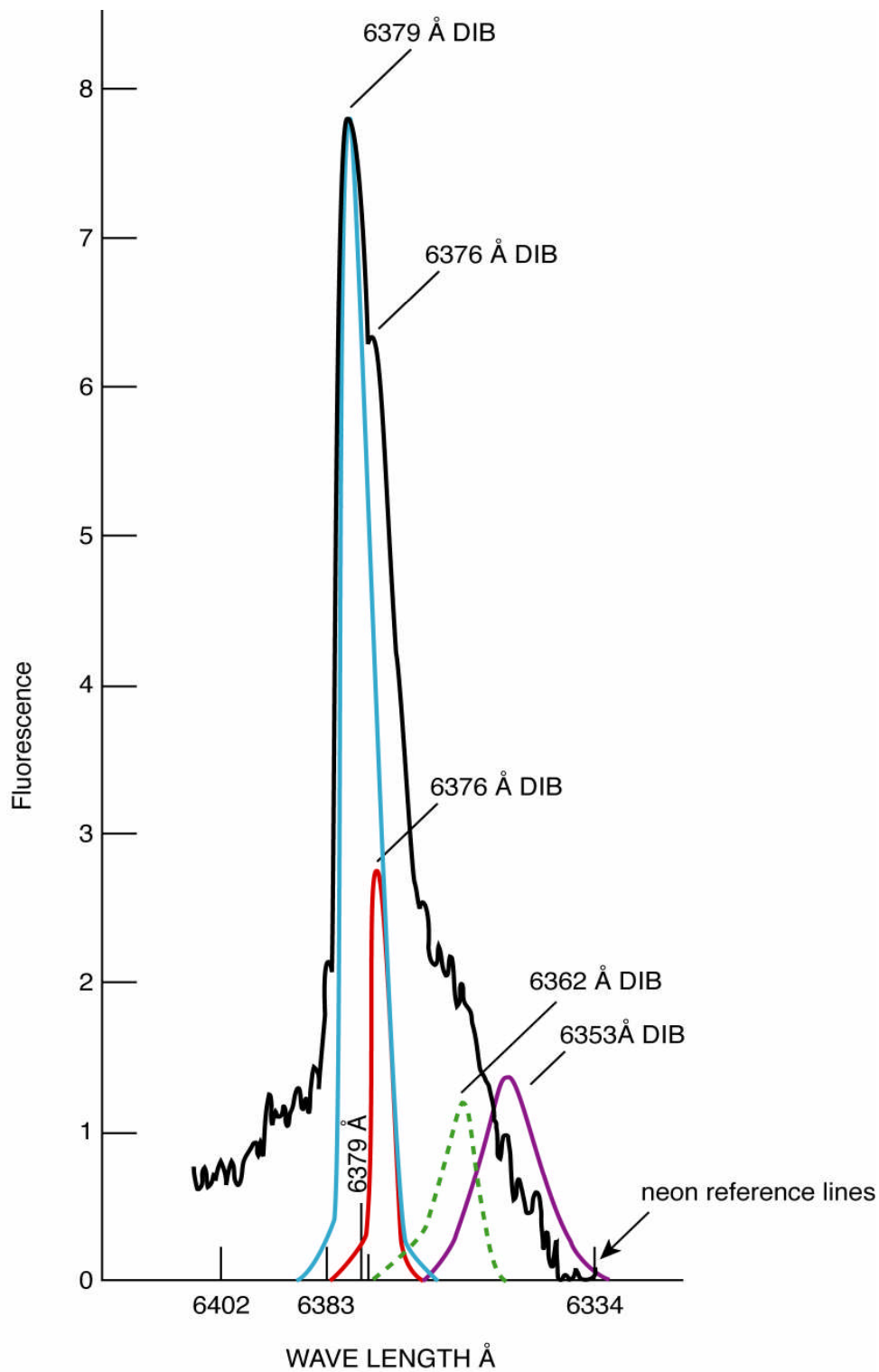


Figure 4. MgTBP in Shpolskii matrix at 77K, showing a lab band at 6379Å, which encompasses DIBs $\lambda\lambda$ 6379, 6376, 6362 and 6353

Author's lab data superimposed with astronomical data.

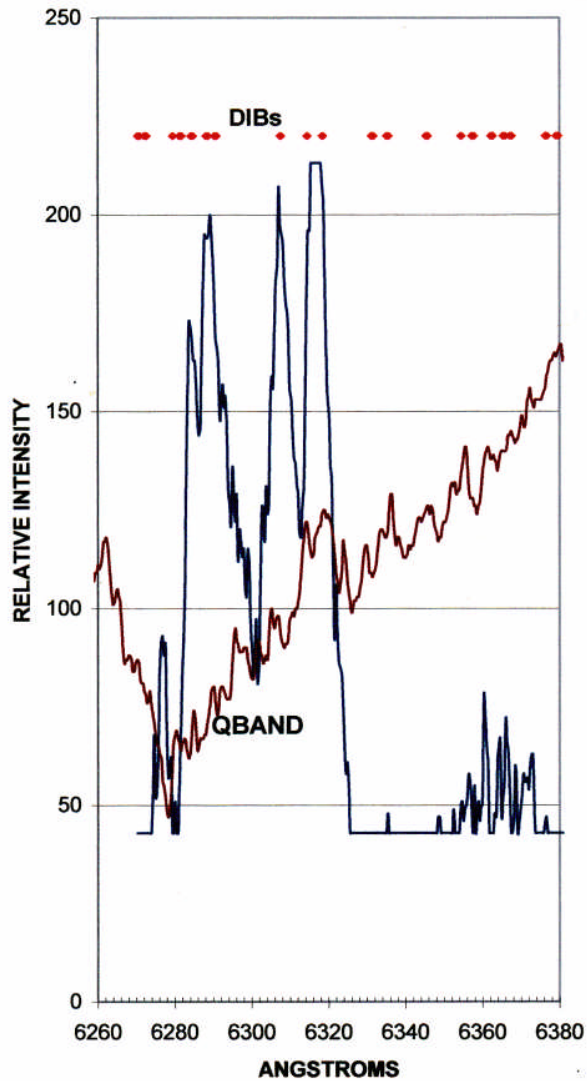


Figure 5. The superposition of two spectral lab bands (using rescanned data by David Weinkle). Note: the Q-band in absorption as well as an emission spectrum. The Q-band illustrates the superposition of an inhomogeneously broadened Q-band, plus a narrow Shpolskii band in the 6284Å region.

Spectral plates from author's data set.

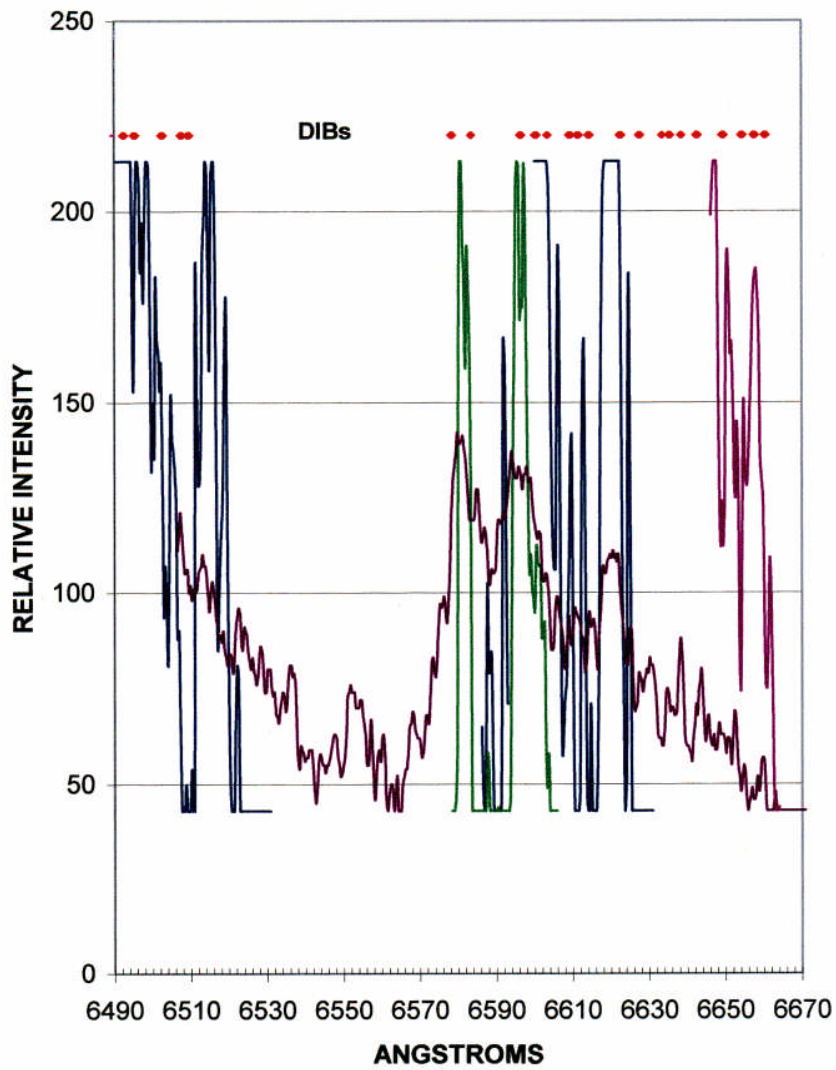


Figure 6. Six individual, superimposed Shpolskii spectral scans.
 Note: the overlap of some of the individual spectral lines.
 Also shown are the relevant, corresponding DIBs.
 Spectral Data from author's data set.

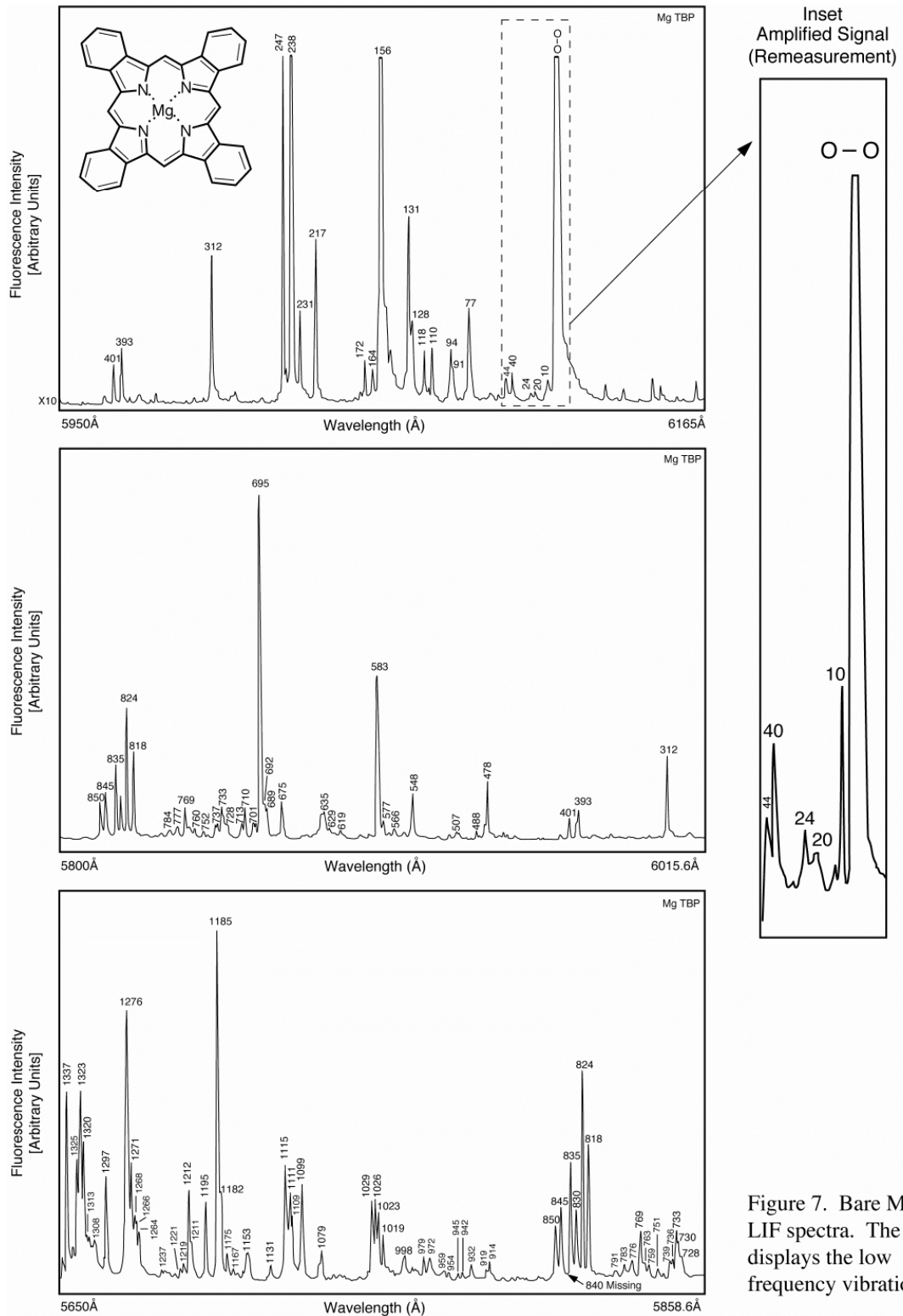


Figure 7. Bare MgTBP LIF spectra. The inset displays the low frequency vibrations.

This commissioned data was supplied by Dr. Don Brumbaugh

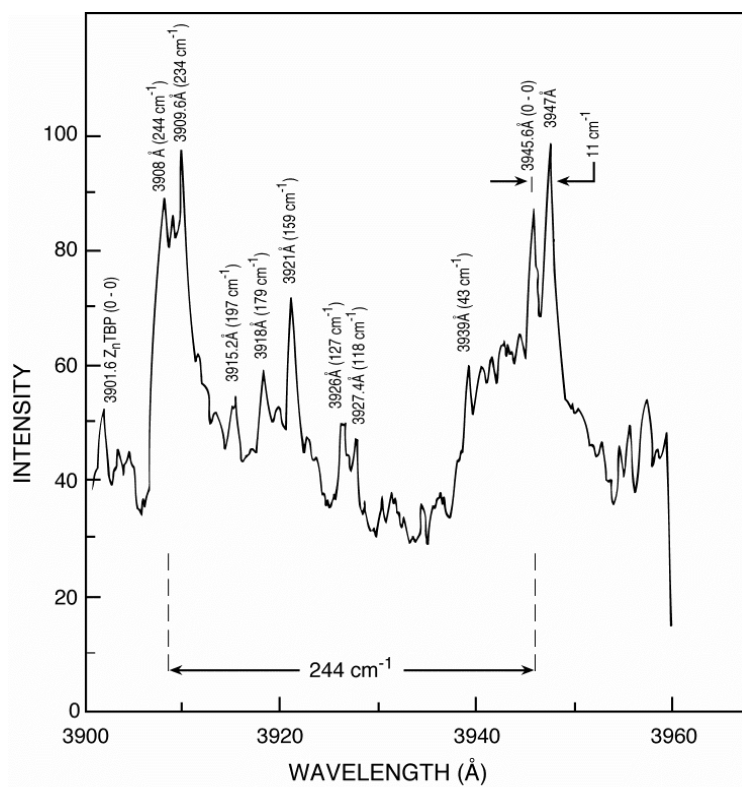


Figure 8a

The $S_2 \leftarrow S_0$ transitions (Soret region) of "bare" MgTBP. From Dr. Uzi Even

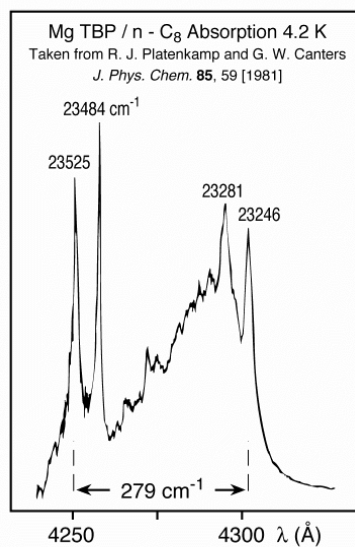
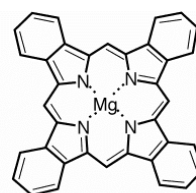


Figure 8b

The Soret band of MgTBP/n-C₈, at 4.2K [7].

Normalized Transmission (linear scale) vs Freq.

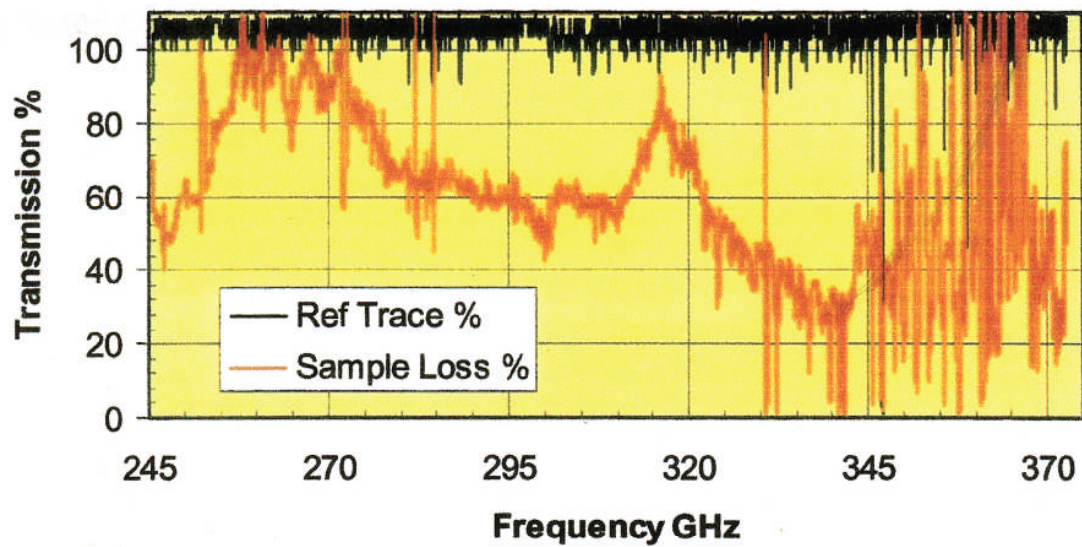


Figure 9. Microwave room temperature absorption measurement of MgTBP. The peak of its absorption is at 341 GHz. The latter value was confirmed by measuring its second harmonic at about 680 GHz. This graph was kindly provided by Dr. P.H. Siegel.

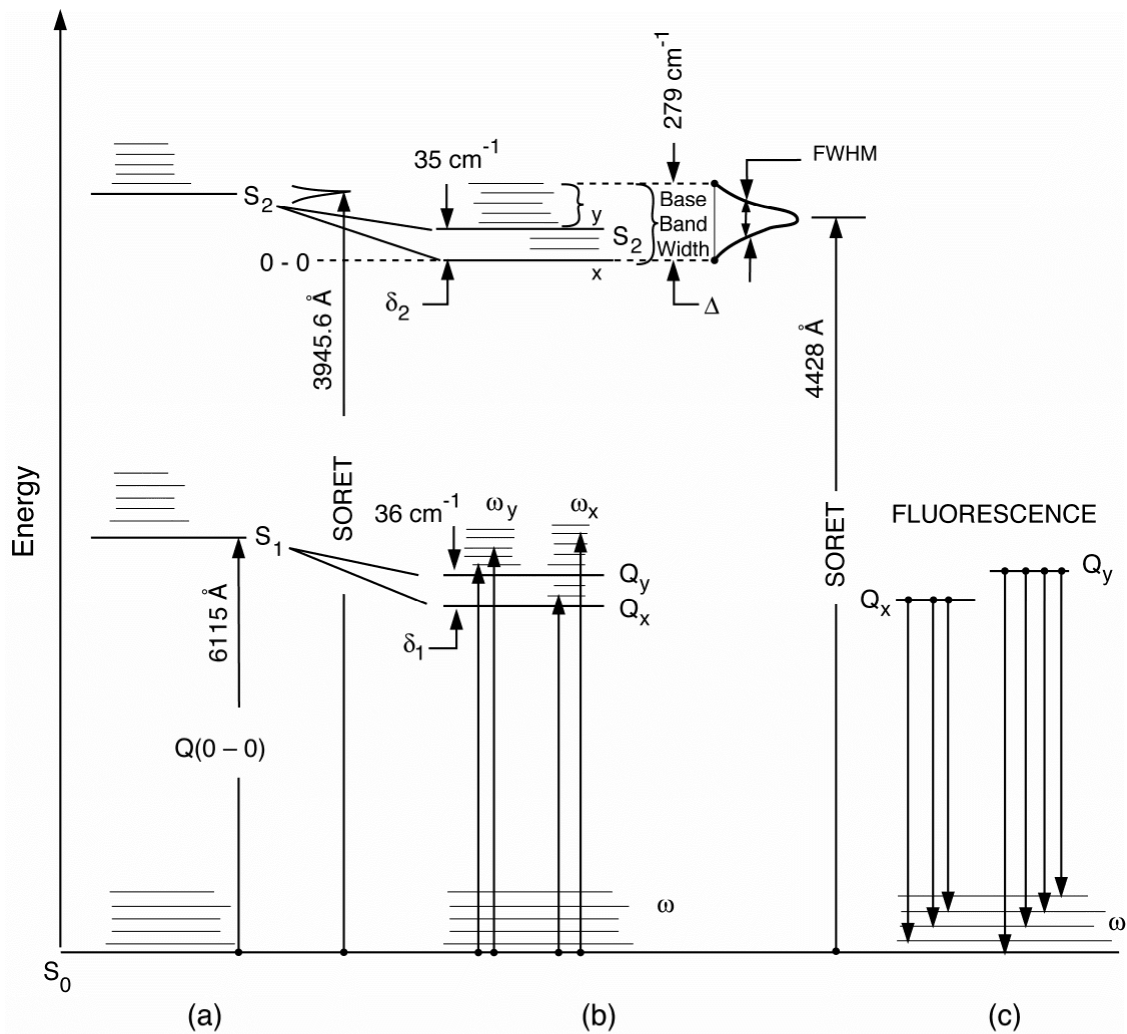


Figure 10. Schematic energy level diagram, showing vibronic transitions in absorption and in emission for MgTBP. Note: the transition from the "bare" state to the matrix and the splitting of the S_1 and S_2 states. Also note the Soret bands in the bare and in the matrix configuration.

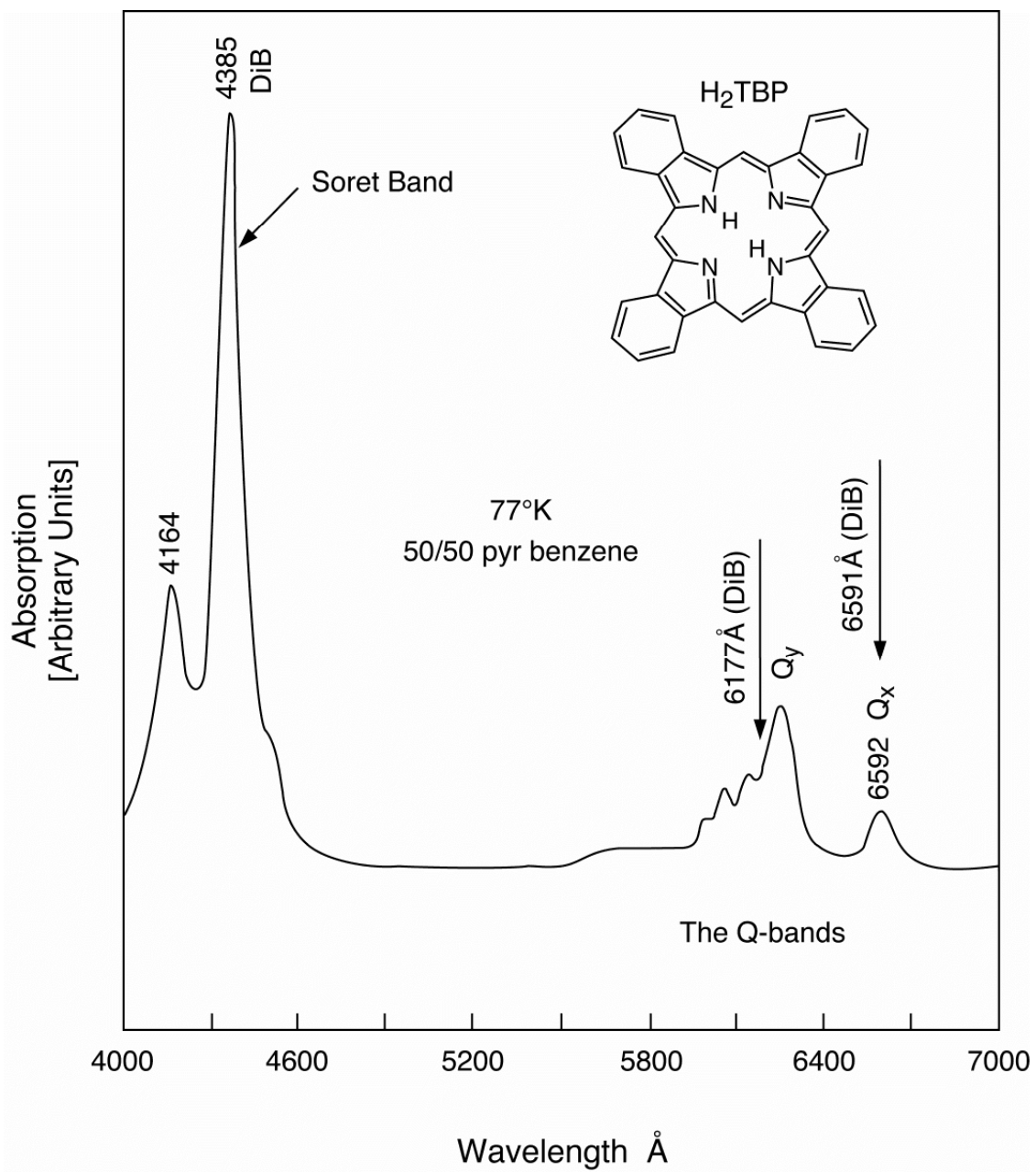


Figure 11. Non-Shpolskii lab absorption spectrum of H₂TBP at 77K.
 Note: the position of the 4385Å Soret band and the double Q-bands.
 Author's lab data.

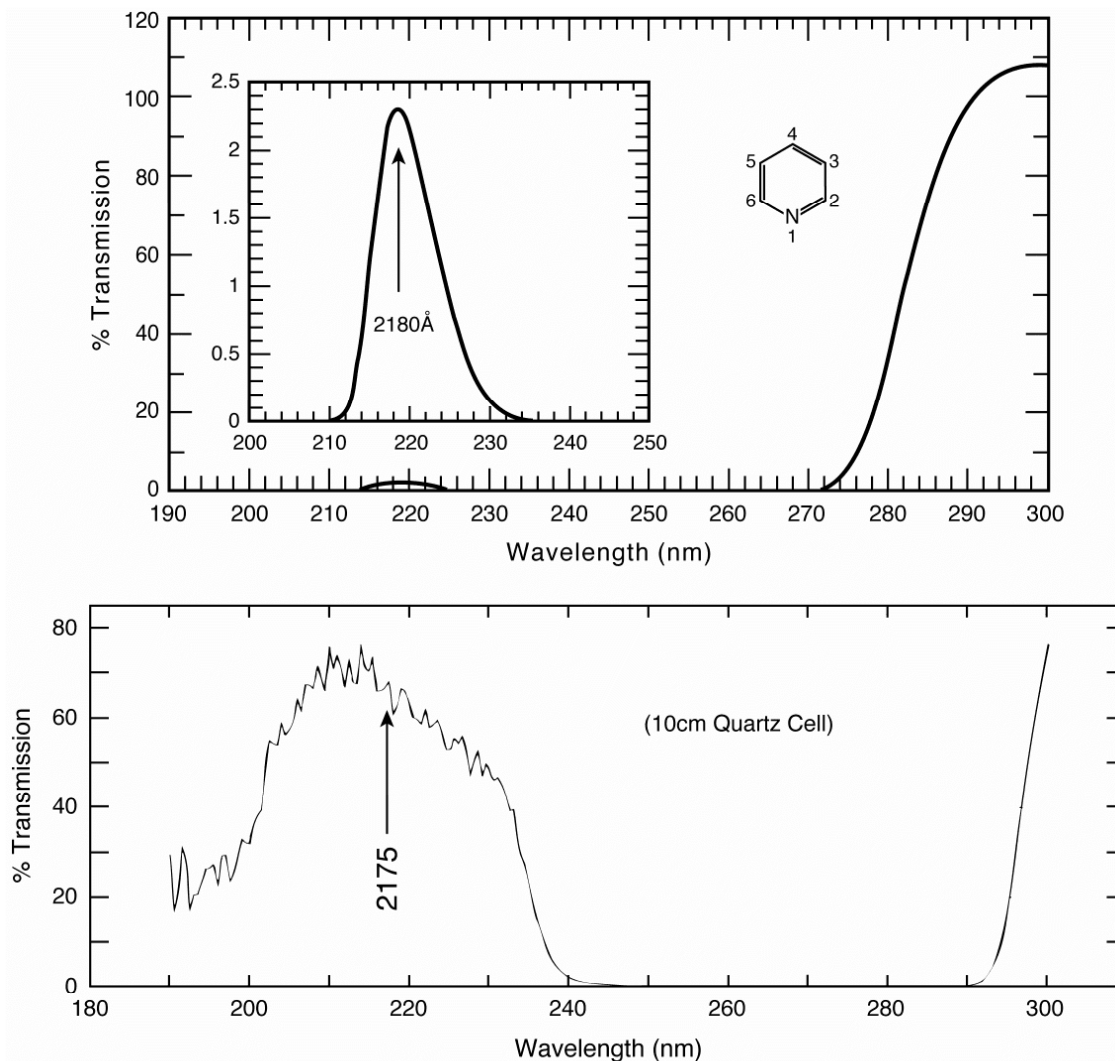


Figure 12. The UV transmission spectra of highly diluted pyridine in an octane solvent, at room temperature, at two different concentrations.
Author's lab data.

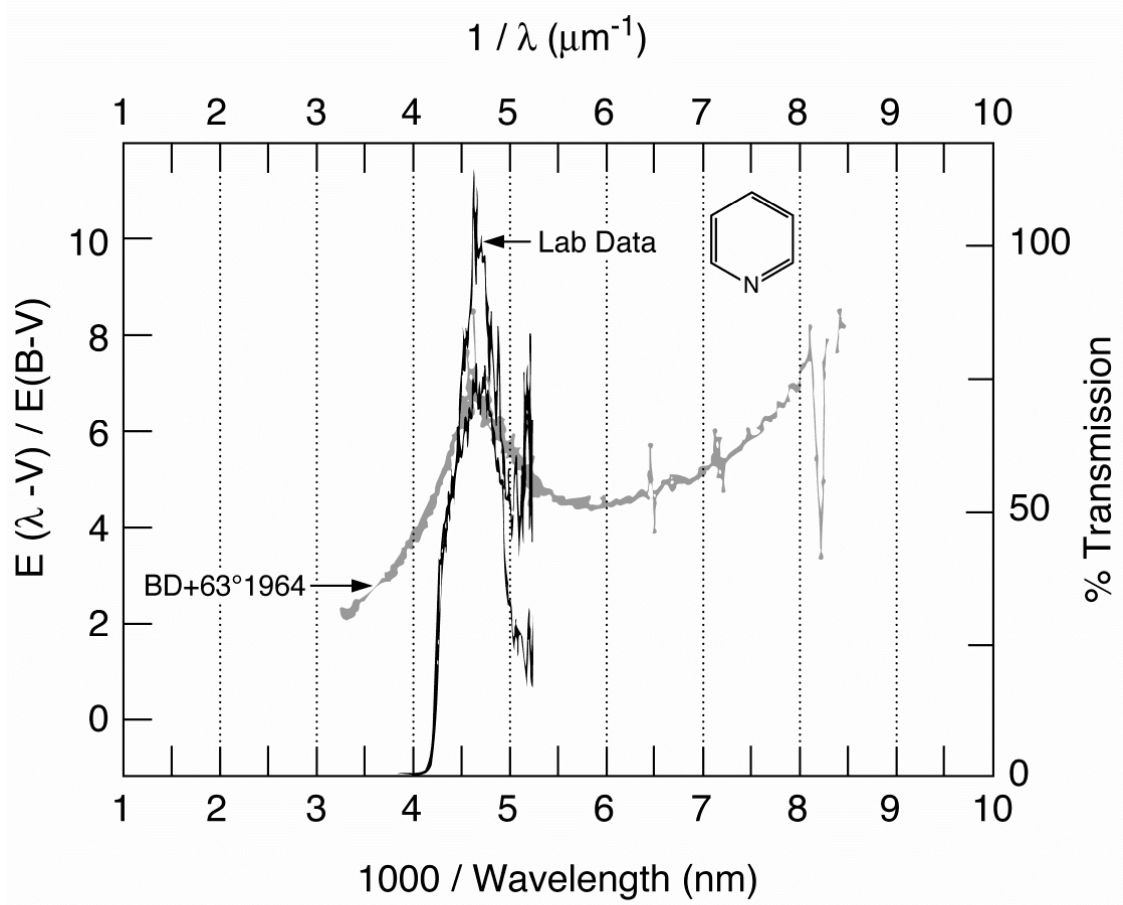


Figure 13. The superposition of the pyridine lab spectrum and a typical UV bump.

Author's lab data.

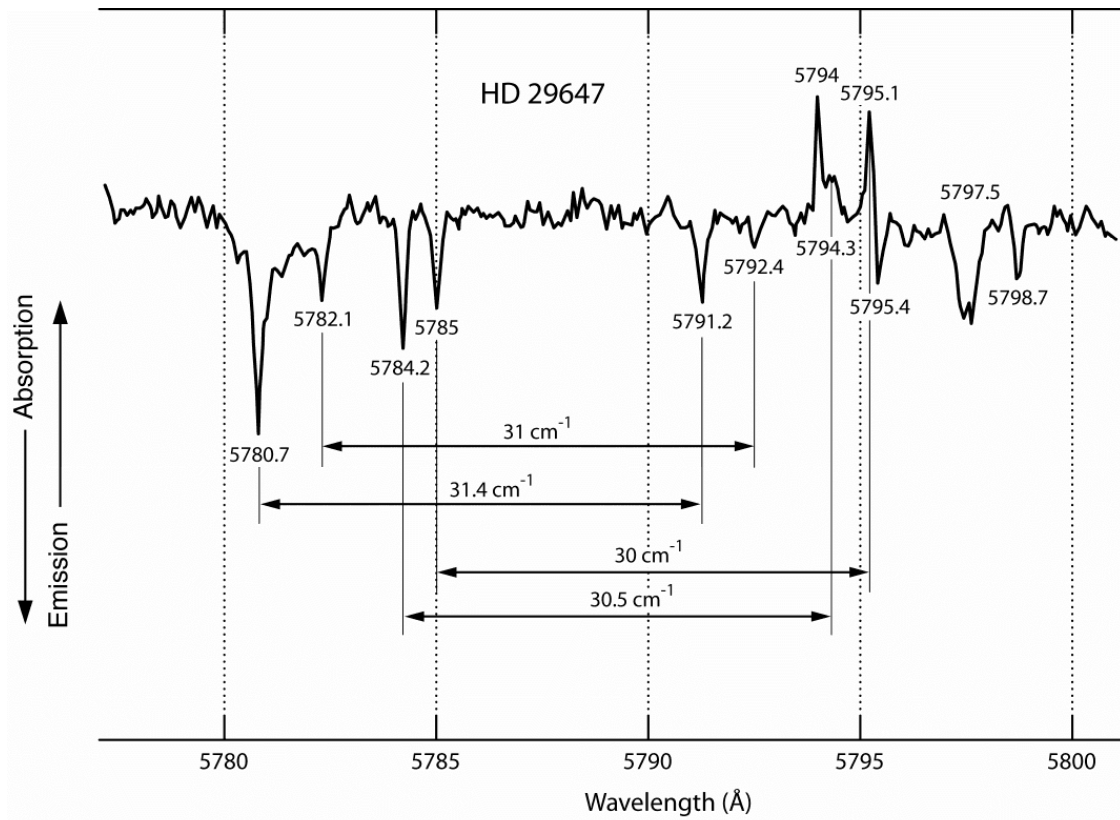


Figure 14. DIBs in HD29647. This graph was adapted from original data supplied by Dr. C.G. Seab. See text for interpretation.

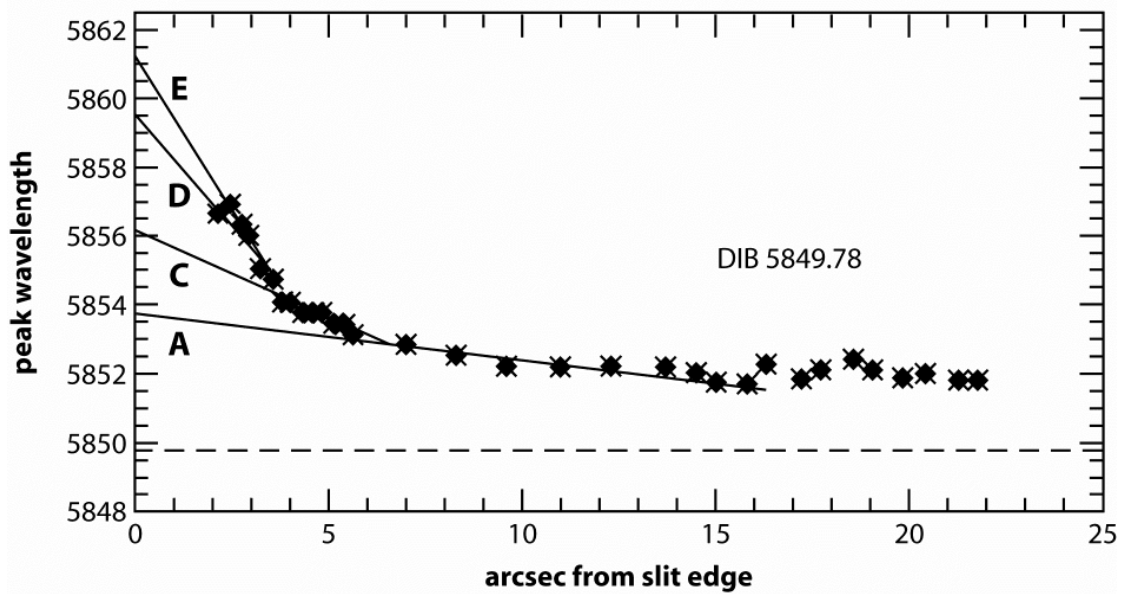
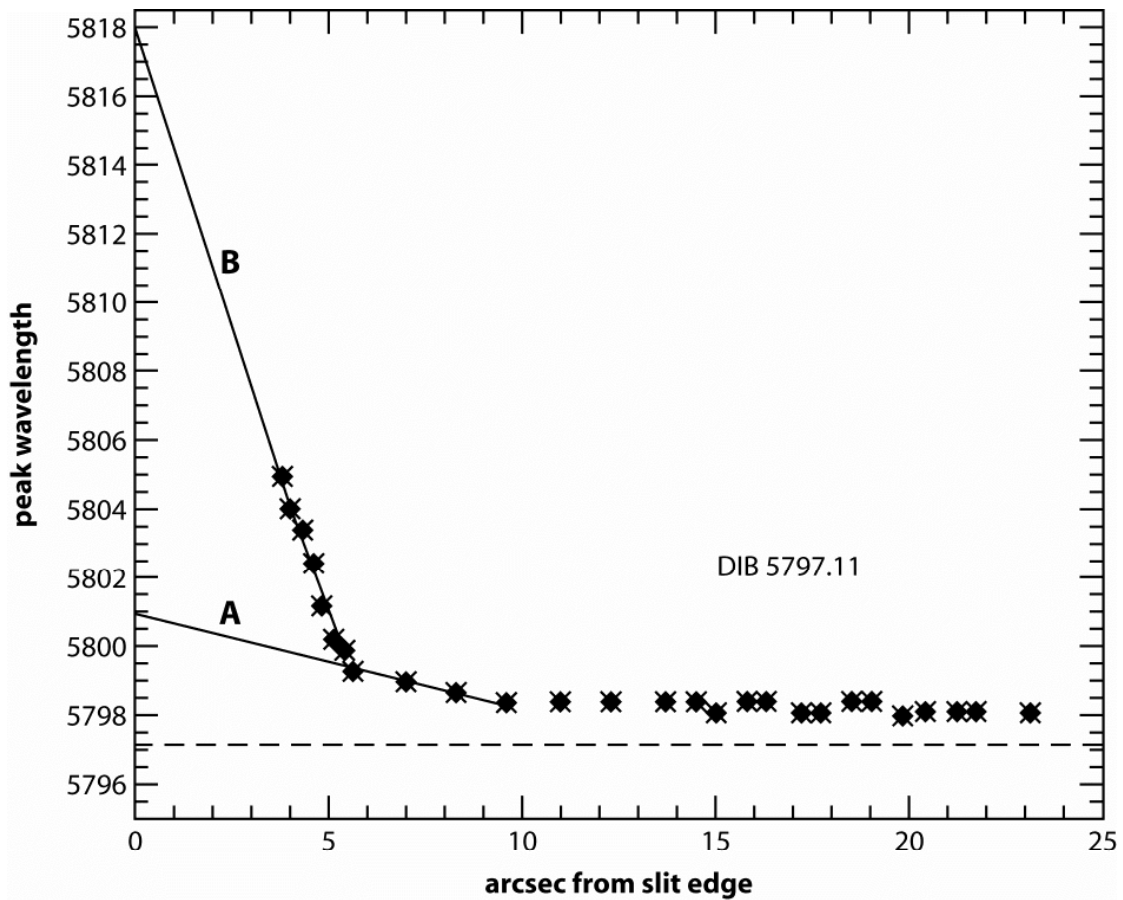


Figure 15. Adapted reproduction of Fig 9. from Van Winckel et al. [87]. The extrapolations from the data generate lines A-E (refer to text for implications)

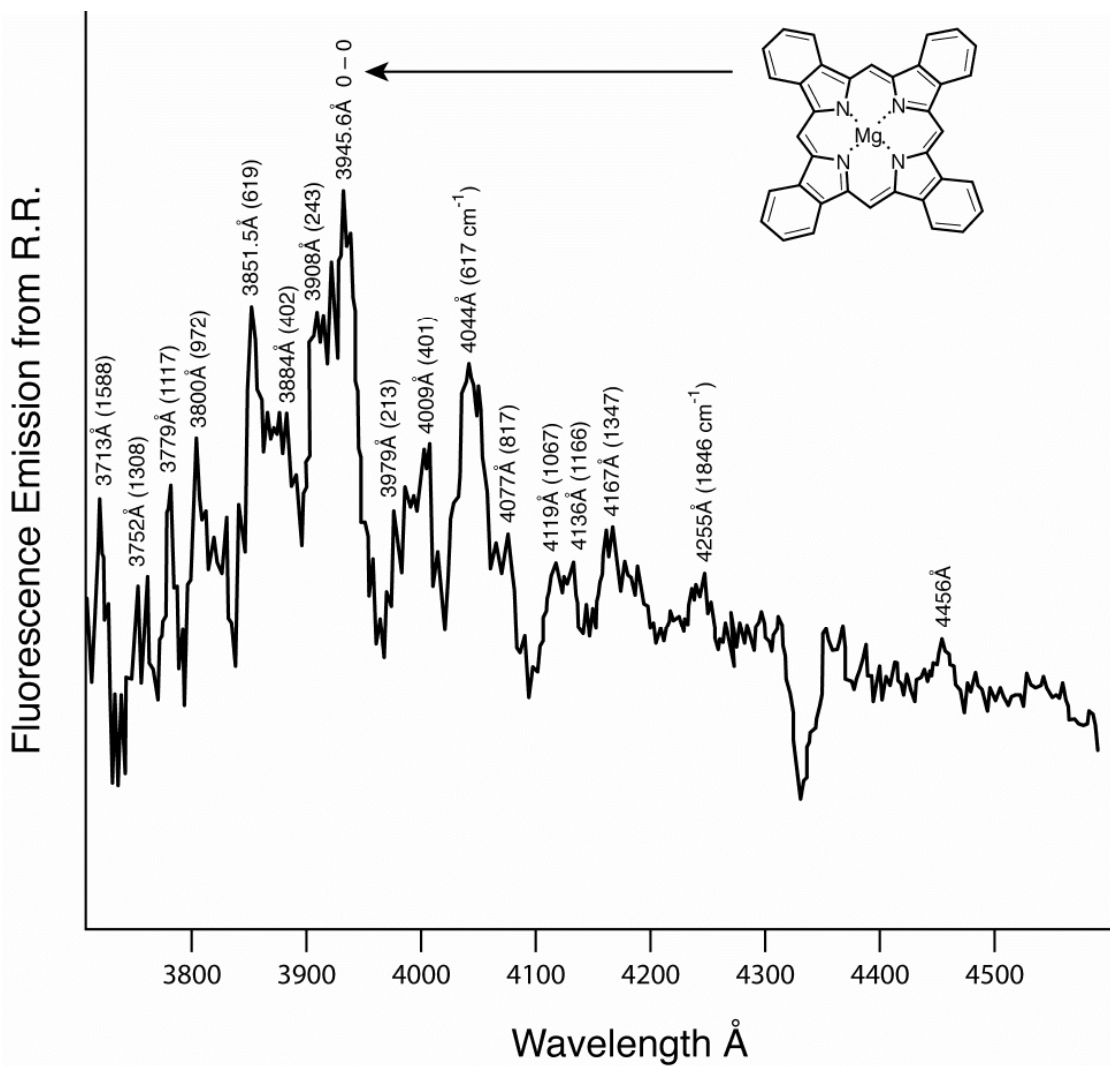


Figure 16. Adapted reproduction from Schmidt et al. [93]. The peaks indicate the fluorescence excitation spectrum associated with MgTBP. Assigned vibrational frequencies are indicated at each peak.

Peaks of published data measured by author. See text for implications.

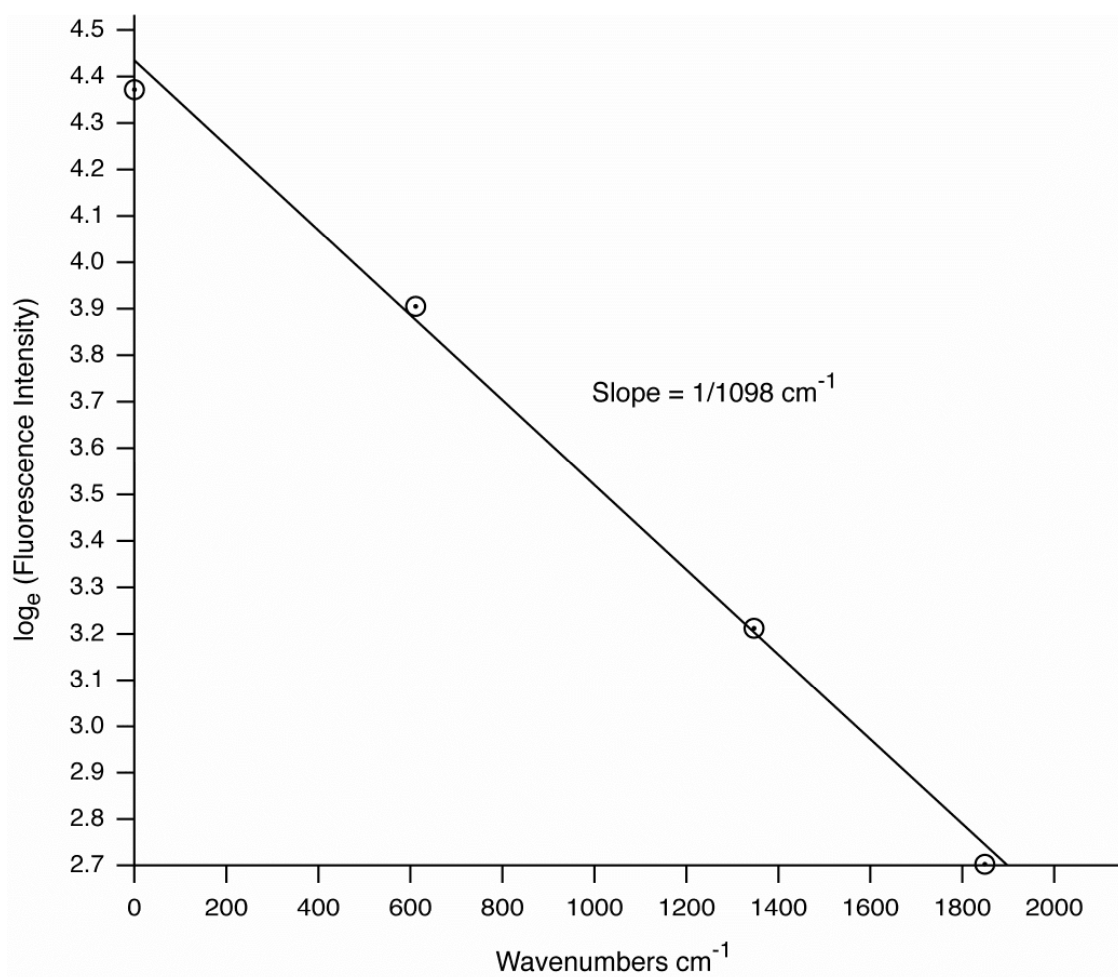


Figure 17. A plot of the log (intensity of fluorescence emission spectrum) vs. excitation energy above the ground state, utilizing the peak intensities of the hot bands (for $\lambda \geq 3945.6\text{\AA}$).

Figure 1. Dipyridyl magnesium tetrabenzoporphyrin ($\text{MgC}_{46}\text{H}_{30}\text{N}_6$).

Figure 2. Energy (in cm^{-1}) level diagram (to scale) of “sites” of MgTBP in matrices of n-octane and octane/ pyridine mixtures for the S_1 electronic state. Sites I thru V are derived from author’s data. Site VI is derived from [7].

Figure 3. The superposition of the MgTBP lab Soret band and the 4428Å DIB. Superpositioned (red) lab Soret band is from author’s data.

Figure 4. Shpolskii matrix at 77K, showing a lab band at 6379Å, which encompasses DIBs $\lambda\lambda$ 6379, 6376, 6362 and 6353. Author’s lab data superimposed with astronomical data.

Figure 5. The superposition of two spectral lab bands (using rescanned data by David Weinkle). Note: the Q-band in absorption as well as an emission spectrum. The Q-band illustrates the superposition of an inhomogeneously broadened Q-band, plus a narrow Shpolskii band in the 6284Å region. Spectral plates from author’s data set.

Figure 6. Six individual, superimposed Shpolskii spectral scans. Note: the overlap of some of the individual spectral lines. Also shown are the relevant, corresponding DIBs. Spectral Data from author’s data set.

Figure 7. Bare MgTBP LIF spectra. The inset displays the low frequency vibrations. This commissioned data was supplied by Dr. Don Brumbaugh

Figure 8a. The $S_2 \leftarrow S_0$ transition (Soret region) of “bare” MgTBP. From Dr. Uzi Even

Figure 8b. The Soret band of MgTBP/n-C₈, at 4.2K [7].

Figure 9. Microwave room temperature absorption measurement of MgTBP. The peak of its absorption is at 341 GHz. The latter value was confirmed by

measuring its second harmonic at about 680 Ghz. This graph was provided by Dr. P.H. Siegel.

Figure 10. Schematic energy level diagram, showing vibronic transitions in absorption and in emission for MgTBP. Note: the transition from the “bare” state to the matrix and the splitting of the S_1 and the S_2 states. Also note the Soret bands in the bare and in the matrix configuration.

Figure 11. Non-Shpolskii lab absorption spectra of H_2TBP at 77K. Note: the position of the 4385Å Soret band and the double Q-bands. Author’s lab data.

Figure 12. The UV transmission spectrum of highly diluted pyridine in an octane solvent, at room temperature, at two different concentrations. Author’s lab data.

Figure 13. The superposition of the pyridine lab spectrum and a typical UV bump. Author’s lab data.

Figure 14. DIBs in HD29647. This graph was adapted from original data supplied by Dr. C.G. Seab. See text for interpretation.

Figure 15. Adapted reproduction of Fig. 9 from Van Winckel et al. [87]. The extrapolations from the data generate lines A-E (refer to text for implications).

Figure 16. Adapted reproduction from Schmidt et al. [93]. The peaks indicate the fluorescence excitation spectrum associated with MgTBP. Assigned vibrational frequencies are indicated at each peak. Peaks of published data were measured by author. See text for implications.

Figure 17. A plot of the log (intensity of fluorescence emission spectrum) vs. excitation energy above the ground state, utilizing the peak intensities of the hot bands (for $\lambda \geq 3945.6 \text{ \AA}$).